# NONUNIFORM FLOW OVER A THERMAL TRANSIENT ANEMOMETER

Ву

James Leung

## A THESIS

Submitted to
Michigan State University
in partial fulfillment of the requirements
for the degree of

Mechanical Engineering – Master of Science

2018

#### **ABSTRACT**

# NONUNIFORM FLOW OVER A THERMAL TRANSIENT ANEMOMETER

By

#### James Leung

An experiment and a simulation have been created to determine if a Thermal Transient Anemometer (TTA) has the capability to measure a nonuniform fluid flow and to output an appropriate average uniform flow. A frame was created with 23 cells that holds a tungsten sensing wire that was heated with an electrical current and cooled with a passing flow. The TTA was then simulated, using an energy balance equation as a basis, to test with more nonuniform flows.

The source of axial heat transfer caused the TTA to cool slower with a nonuniform flow than an equivalent uniform flow at an averaged flow speed. The percent the nonuniform flow differed from this equivalent averaged flow changed based was on two main factors of the flow; if any region of the flow existed at low speeds and if the flow has large gradients. With this in mind the TTA will still have a usable operational condition. Namely, if the flow is not at a low speed and if it has a modest gradient.

#### **ACKNOWLEDGEMENTS**

This thesis was made possible due to the collective assistance from this author's professors and colleagues at Michigan State University. Special thanks to my advisors, Dr. John Foss and Dr. James Klausner for giving me this chance and guide me through this process.

I would also like to thank Paul Sandherr, Kelvin Randhr, Thomas Stuecken and Claus Buchhhoz for their assistance in this project. Their help was greatly needed for this difficult task.

Finally, I would like to thank my family and close friends that made any difficulties that may arise bearable.

# TABLE OF CONTENTS

LIST OF TABLES	vi
LIST OF FIGURES	vii
KEY TO SYMBOLS AND ABBREVIATIONS	X
1.0 <b>Introduction</b>	1
1.1 Motivation	1
1.2 Previous Work	2
1.3 Goals	2
2.0 The TTA System	4
2.1 Design of the TTA	
2.2 TTA Frame Fabrication	
2.3 Sensing Wire Characteristics	13
3.0 Numerical Simulation of TTA Thermal Effects	
3.1 Equation Derivation	
3.2 Heat Convection	
3.3 Boundary Condition	
3.4 Simulation	
3.5 Verification	19
4.0 Experimental Investigation	
4.1 Test Facility	
4.2 Hot-Wire Probe Anemometry	
4.3 CTA Calibration	
4.4 TTA Frame Calibration	35
5.0 Evaluation of the Numerical Simulation	37
6.0 Nonuniform Velocity Profile	
6.1 Experimental Procedure for the Non-uniform Velocity Distribution	
6.2 Experimental Results	
6.3 Simulation Comparison	43
7.0 Simulations of Non-Uniform Velocity Profiles	
7.1 Simulated Temperature Distributions for Nonuniform Velocity	
7.2 Simulated Mean Velocity Prediction for Linear Variation in Velocity	
7.3 Convective Heat Transfer	53
8.0 Conclusion	56

APPENDICES	57
APPENDIX A. CTA Calibrations at Low Speed	58
APPENDIX B. Calibration Curves for the Rest of the TTA	
APPENDIX C. Derivation of Equations 31 and 32	62
REFERENCES	65

# LIST OF TABLES

Table 7.1. Linear Flow Data	52	2
Table /.1. Linear Flow Data	5	2

# LIST OF FIGURES

Figure 1.1. Example Engine Cooling System Obtained from ClearMechanic.com [4]	.1
Figure 2.1. Completed Frame Full View	.5
Figure 2.2. Close Up of Completed Frame and Components	.6
Figure 2.3. Garolite A	.8
Figure 2.4. Garolite B	.8
Figure 2.5. Garolite C	.9
Figure 2.6. Garolite D	.9
Figure 2.7. Garolite E	0
Figure 2.8. Garolite Inside an Inside Cell in the Frame	0
Figure 2.9. Garolite Inside a Border Cell in the Frame	ւ 1
Figure 2.10. Partially Wired TTA	ւ 1
Figure 2.11. Fully Wired TTA	. 2
Figure 2.12. Terminal Block1	.2
Figure 2.13. Diagram of Securing the Wire	.3
Figure 3.1. Energy Budget for a Wire Segment	.5
Figure 3.2. Comparing Exponential Decay to Experimental Nondimensional Resistance	20
Figure 3.3. Comparing Numerical Solution to Exact Solution for a Wire with an Initial Linear Temperature Profile	22
Figure 3.4. Comparing Numerical Solution to Exact Solution for a Wire with an Initial Parabolic Temperature Profile	23
Figure 4.1. Side View of TTA Testing Facility	25
Figure 4.2. Front View of TTA Testing Facility	26

Figure 4.3. TTA Testing Facility with TTA Installed	27
Figure 4.4. Frontal View with Honeycomb	28
Figure 4.5. TTA Testing Facility with No Air Bleed	29
Figure 4.6. TTA Testing Facility with Large Amount of Bleed	30
Figure 4.7. View of Testing Facility with Radiator Installed	31
Figure 4.8. View of Testing Facility with Radiator and Shroud Installed	32
Figure 4.9. Image of the Hot Wire Probe.	33
Figure 4.10. Image of the Hot Wire Probe Close Up	33
Figure 4.11. Hot Wire Probe Calibration Facility	34
Figure 4.12. Hot Wire Probe Calibration	35
Figure 4.13. Example of a Row Calibration of the TTA	36
Figure 5.1. Comparison of τ Between Row 1 to Simulation	37
Figure 5.2. Comparison of τ Between Row 2 to Simulation	38
Figure 5.3. Comparison of τ Between Row 3 to Simulation	38
Figure 5.4. Comparison of τ Between Row 4 to Simulation	39
Figure 5.5. Comparison of τ Between Row 5 to Simulation	39
Figure 5.6. Comparison of τ Between Row 6 to Simulation	40
Figure 6.1. TTA Testing Facility with Cloth Gradient Over the Face	42
Figure 6.2. Nonuniform Flow Over the Row 3, Cell 3 Measured with Hot Wire Probe	43
Figure 7.1. Transient Cooling Under Uniform Flow, Speed of 10 m/s	46
Figure 7.2. Transient Cooling with Linear Variation in Velocity, U <sub>avg</sub> =10 m/s b=10 m/s	47
Figure 7.3. Transient Cooling with Parabolic Variation in Velocity, Shown in Equation 37	48

Figure 7.4. Transient Cooling with Sinusoidal Variation in Velocity, Shown in Equation 38	49
Figure 7.5. Comparison of Simulated Nondimensional Resistance to Exponential Decay with Linear Velocity Profile, Equation 36	50
Figure 7.6. Comparison of Simulated Nondimensional Resistance to Exponential Decay with Parabolic Velocity Profile, Equation 37	50
Figure 7.7. Comparison of Simulated Nondimensional Resistance to Exponential Decay with Sinusoidal Velocity Profile, Equation 38	51
Figure 7.8. Suggested Operational Range of the TTA	52
Figure 7.9. Suggested Operational Range of the TTA Zoomed In	53
Figure 7.10. Initial Convection Coefficient	54
Figure 7.11. Wire Temperature Distribution with Respect to Time	55
Figure 7.12. Comparison of Temperature Decay Between a Non-Uniform Velocity Profile to the Average Uniform Velocity Profile	55
Figure A.1. CTA Probe Calibration at Low Air Speeds	58
Figure A.2. Row 1 Calibration	58
Figure A.3. Row 2 Calibration	59
Figure A.4. Row 4 Calibration	59
Figure A.5. Row 5 Calibration	60
Figure A.6. Row 6 Calibration	60

# KEY TO SYMBOLS AND ABBREVIATIONS

# **KEY ABBREVIATIONS**

# CTA Constant Temperature Anemometer

# TTA Thermal Transient Anemometer

# ROMAN SYMBOLS

$A_c$	Cross sectional area of the wire	<i>(m)</i>
$C_p$	Specific heat of wire	$\left(\frac{J}{kg-K}\right)$
D	Diameter of wire	( <i>m</i> )
E	Voltage	(E)
$\boldsymbol{G}$	Nondimensional term	
Н	Height of a cell	( <i>m</i> )
h	Heat convection coefficient	$\left(\frac{w}{mk}\right)$
I	Current through the wire	( <i>A</i> )
k	Thermal conductivity of wire	$\left(\frac{kg\cdot m}{K\cdot s^3}\right)$
L	Length of wire	( <i>m</i> )
Nu	Nusselt Number	
Pr	Prandlt Number	
q <sup>·</sup>	Heat transfer over small wire segment	$\left(\frac{kg}{s^3}\right)$
R	Resistance of wire	$(\Omega, ohm)$
Re	Reynolds Number	
T	Temperature	(°C)
t	Time	(s)

UAir Speed $\left(\frac{m}{s}\right)$ xPosition along the wire(m)

#### **GREEK SYMBOLS**

 $\delta \tau$ Percent difference between measured and simulated  $\tau$  $\delta V$ Percent difference between expected and simulated auResistivity of wire  $(\Omega \cdot m)$ γ Nondimensional Temperature or Nondimensional Resistance Θ Kinematic Viscosity ν Density of wire ρ (s) τ Time Constant  $({}^{\circ}C)^{-1}$ ζ Temperature Coefficient of Resistance

#### SUBSCRIPTS/SUPERSCRIPTS

a Property at ambient air condition

avg Average of velocity profile

expected Value achieved by using the calibration to predict

film Property at film condition

linear Air flow with a linear velocity profile

ref Reference Conditions

parabolic Air flow with a parabolic velocity profile

simulated Value achieved by using numerical solution

sinusoidal Air flow with a parabolic sinusoidal profile

w Property of wire

#### 1.0 Introduction

#### 1.1 Motivation

Internal combustion engines require heat removal for safe operation. The exothermic reaction taking place in the combustion chamber coupled with the mechanical friction generate heat that needs to be evacuated in order to maintain high performance without compromising reliability. This limits the engine output to the performance of the cooling system. The cooling system is comprised of a radiator, shroud, fan, and cooling fluid. Moving the heat from coolant to air is the primary function of the radiator which increases the heat transferred from the engine to the cooling system. A modern cooling system is shown in Figure 1.1.

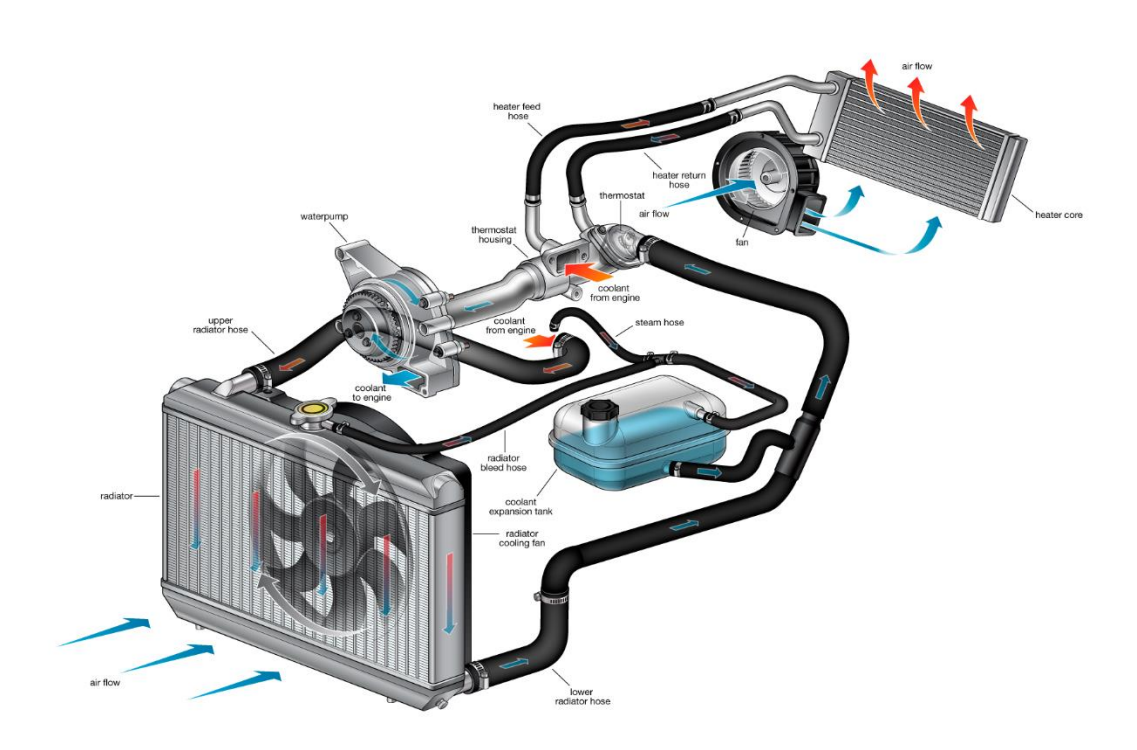


Figure 1.1. Example Engine Cooling System Obtained from ClearMechanic.com [4]

There are many approaches to improve the cooling system; optimizing the shroud design to improve the uniformity of the air flow across the radiator is one such strategy. This requires understanding the air flow over the radiator. The Thermal Transient Anemometer or TTA was developed to address this objective. The total area at the face of the radiator is subdivided in to measurement cells. The TTA responds to an average velocity at given cells. The TTA was chosen over other designs of anemometers due to the thin design of the TTA, which allows it to fit in between the radiator and the shroud with a relatively low disruption to the air flow.

#### 1.2 Previous Work

The initial development of the TTA was reported by Foss, et al. (2004) [6]. The basic operating principle, described therein, is to determine the average velocity at the face of a cell (U) by measuring the cooling rate of a previously heated sensor wire. The cooling follows an exponential decay of the temperature and hence of the wire's resistance that is proportional to its temperature. Namely

$$\frac{R(t) - R_a}{R(t=0) - R_a} = \exp\left(-\frac{t}{\tau}\right). \tag{1}$$

Hence,  $\tau$  can b used as a measure the cooling rate. From Foss, et al. (2004), the average velocity can be related to  $\tau$  as

$$\frac{1}{\tau} = A + BU^c. \tag{2}$$

Foss, et al (2006) [5] used an elevated ambient temperature and turbulent flow to confirm that the TTA is still accurate at higher temperatures and with turbulence, conditions are expected for a TTA mounted in a vehicle radiator for testing. This thesis builds on the previous works by finding a relationship between a non-uniform air flow and the cooling rate of the sensor wire.

## 1.3 Goals

The two prior TTA publications have not addressed the issue: "what is the effect of a non-uniform velocity at the face of a cell?" The present investigation is to answer this question.

Specifically, if a non-uniform velocity is present at a cell and if the  $\tau$  value is obtained, what is the relationship between the inferred velocity and the spatially averaged velocity at the face of the cell?

#### 2.0 The TTA System

## 2.1 Design of the TTA

An assembled TTA frame is shown in Figure 2.1. The TTA uses tungsten as the sensing wire. It is supported by a metal frame to measure the air speed. The metal frame divides the radiator area into a 4 by 6 grid of cells (ie., smaller areas). Each cell holds a 1.6-meter segment of the sensing wire. A cell on the top right (of the Figure 2.1) was excluded due to design constraints of the testing shroud, leaving 23 cells. The number of cells provide a detailed survey over the radiator with minimally blocking the face of the radiator and without disturbing the flow of air. The sensor wire was connected by a cable to a control unit made by Sakor Technologies Inc., which controls the TTA and sends the data to the user's computer. To collect data, the unit sends an electric current (for a designated time period) to heat the sensor wire it to an elevated temperature. At the end of the designated time period the unit will switch the current to a sensing current (10 mA). The recording A/D converter (100 mV full scale) records the sensor wire resistance during the cooling period. Time zero is set after the after the cooling period when the resistance reaches steady state if there is a high air speed. If there is a high air speed and the resistance exceeds 10 ohms then the time zero is set after the resistance reaches 10 ohms after the cooling period. The cooling process will continue for a set period of time, which it will then produce a time in which the nondimensional resistance will reach  $\exp(-1)$ . This time becomes the value of  $\tau$  which the TTA outputs for the user when calibrating. The significance of  $\tau$  was explained in Section 1.2. There is a linear correlation with resistance and temperature, which will be explored further in Section 2.3. A correlation between the rate of temperature decay and an air speed can be determined after calibration.



Figure 2.1. Completed Frame Full View
Note: The inside dimension of each cell is
0.166 m by 0.274 m

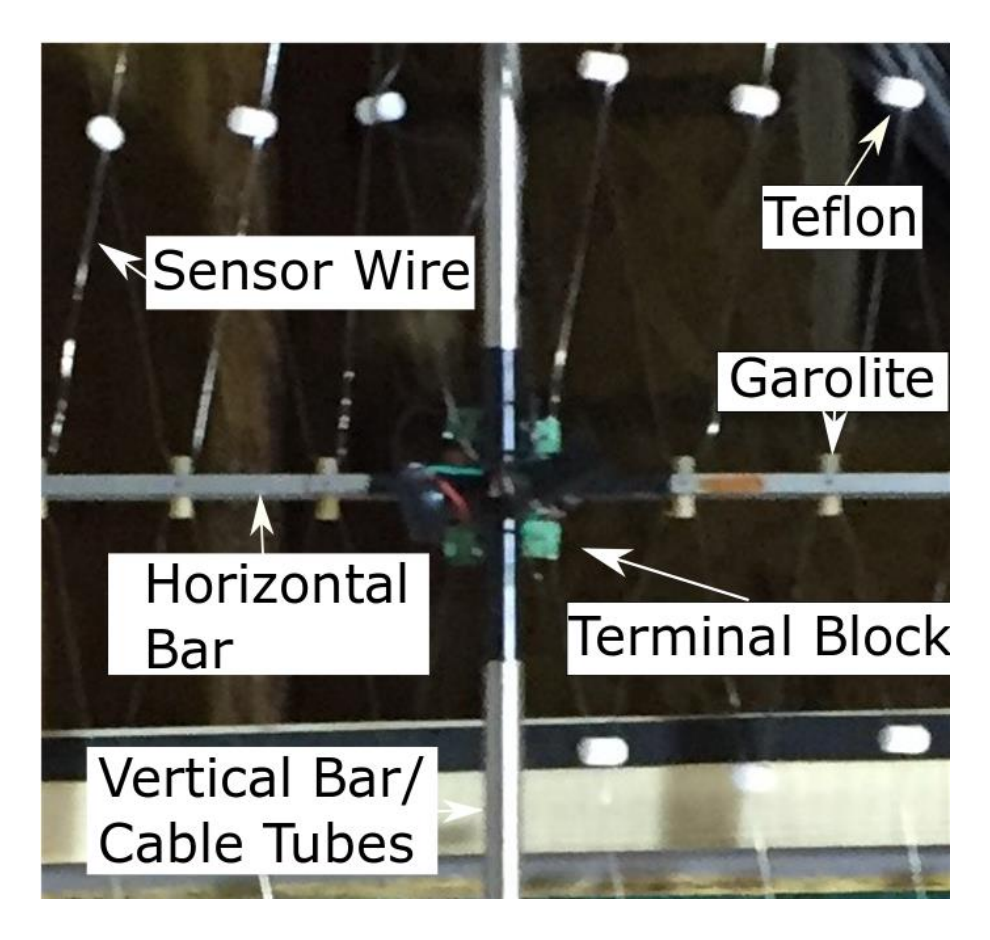


Figure 2.2. Close Up of Completed Frame and Components

#### 2.2 TTA Frame Fabrication

The metal bars used as the structure were machined from stainless steel. Referring to Figure 2.2, the horizontal bars of the frame have holes for Garolite rod inserts to hold the sensor wire. The Garolite electrically insulates the sensor wire from the frame. Garolite is a composite material. It was selected due to its thermal and electrical resistant properties. The Garolite inserts have various designs, dependent on the location on the frame. One version had a hole drilled down the axial center of the Garolite rod. The other designs have a hole radially through the center of the Garolite for the Garolite to be secured on to the frame with a small metal pin and another hole radially near the end to hold the wire. These designs can be seen in Figure 2.3-2.7. The placement of each Garolite piece in a cell can be seen in Figure 2.8 and Figure 2.9. The method of wiring the

cell can be seen in Figure 2.11 with Teflon inserts between the 'x' to prevent conduction radially between the wires. Teflon was used due to the high thermal and electrical resistance and ease of machining. It was not used for the tether points (now insulated by the Garolite) because the Teflon was too soft, and the wire was expected to cut through the Teflon.

An initial and an unworkable configuration for the TTA used stainless steel wire. The cell sizes were selected to provide a 4 x 6 array that covered the project radiator. The location for the Garolite members were set to achieve a resistance of ohms for the cell's ambient temperature resistance. The stainless-steel wire proved unworkable as a result of its insensitivity to increases of temperature: too small of a temperature coefficient of resistance which will be discussed further in Section 2.3. Satisfactory performance was obtained with the replacement wire tungsten. The length (about 1.6 m) and diameter (0.2 mm) were selected to be compatible with the installed Garolite members and to provide an ambient temperature resistance of 2.85 ohms.

The inability to solder directly to tungsten wire presented a substantial problem for the wiring of the frame. (Note that copper plating was used on tungsten wire in earlier versions of the TTA. That plating process is challenging, and it was not attempted in this project.) Plastic coated terminal blocks, shown in Figure 2.12, were used to address this issue. The terminal blocks used metal screw clamps to secure the wire into place. The terminal blocks also providing an electrical connection between a copper wire and the sense wire by soldering the copper wire to a prong, an extension of the clamps, on the terminal block. The terminal blocks' plastic coating prevents electrical conduction to the rest of the frame. The wire was secured as show in Figure 2.13, where the terminal block lays on its side. A copper wire that provides electrical connection was soldered to the extended prongs of the blocks. The copper wire is a part of the Belden Cable used to connect the sense wires to the Sakor Unit. The Belden Cable was chosen because the individual 6 wires,

22-gauge wires, inside the cables were grouped in twisted pairs and the metallic shield over the wires which prevents noise. The Belden Cable was protected from external damage by stainless steel tubes that were welded to vertical bars of the frame.

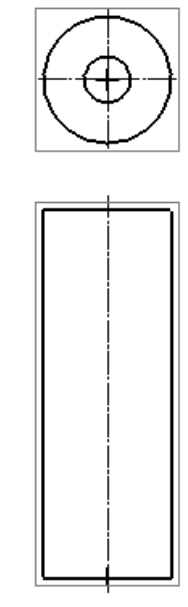


Figure 2.3. Garolite A

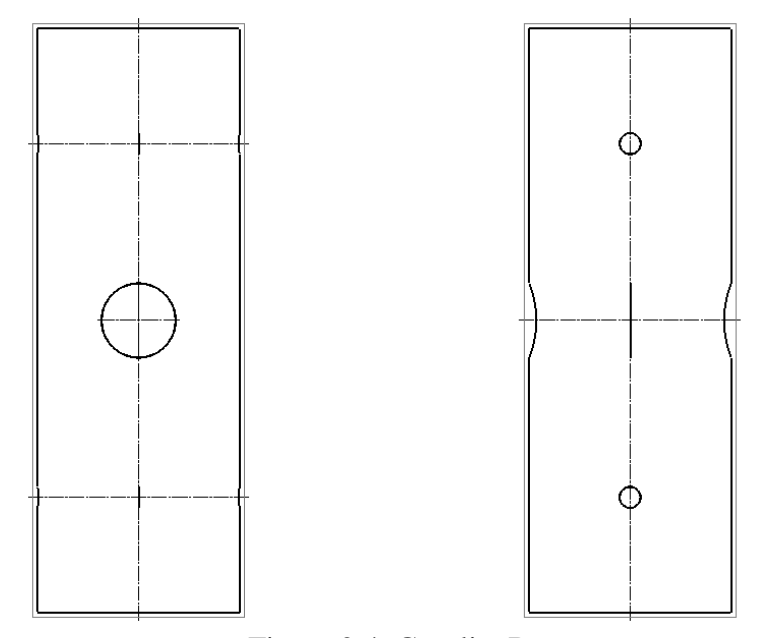


Figure 2.4. Garolite B

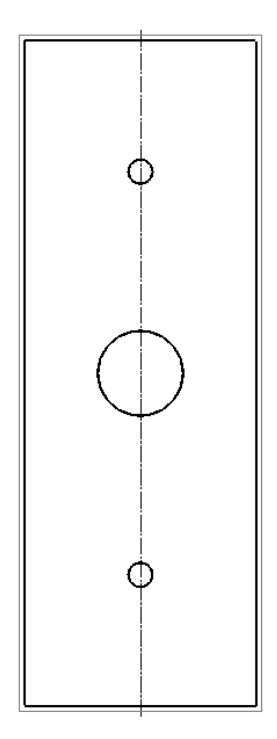


Figure 2.5. Garolite C

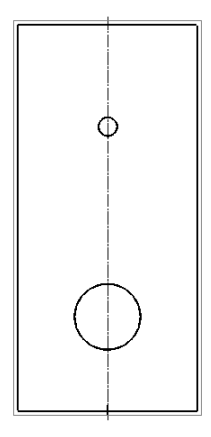


Figure 2.6. Garolite D

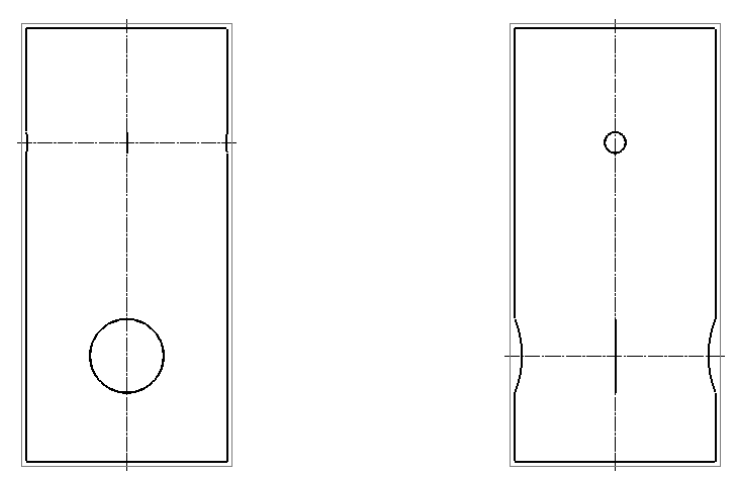


Figure 2.7. Garolite E

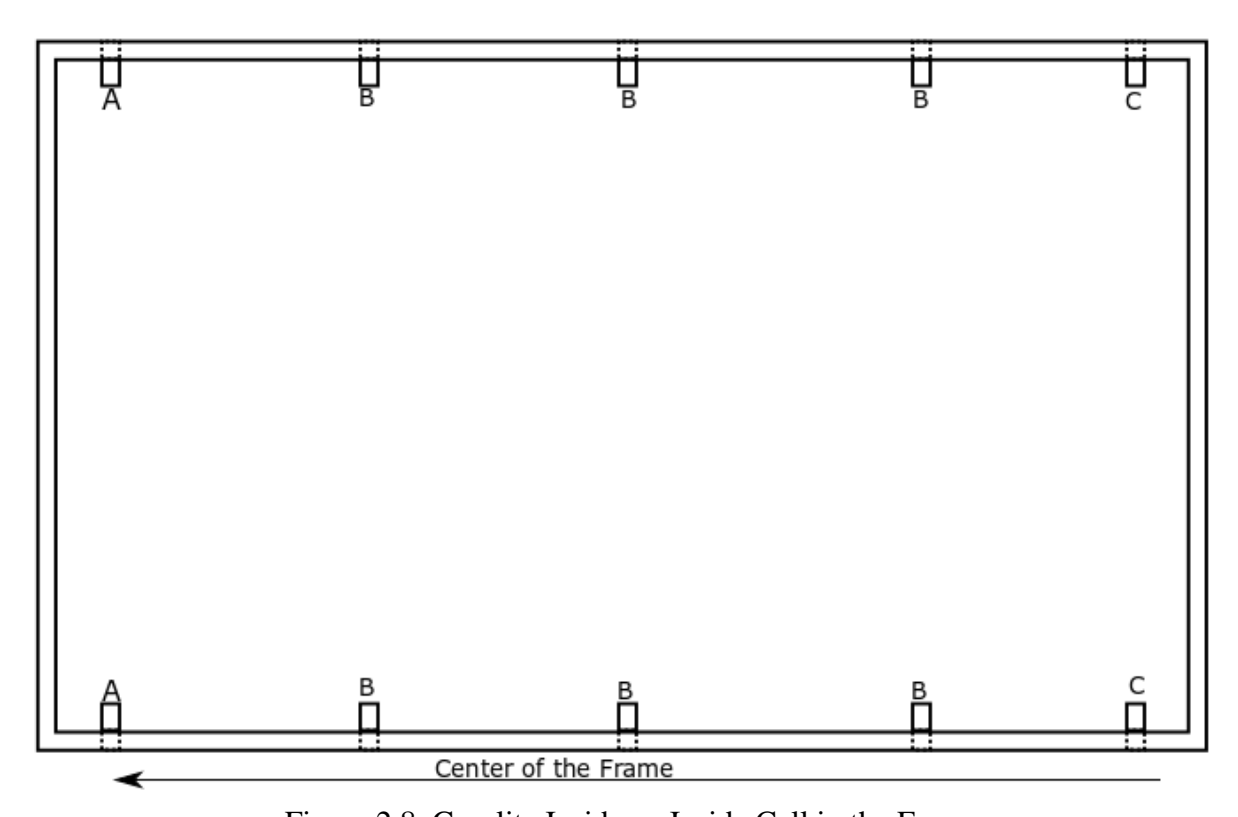


Figure 2.8. Garolite Inside an Inside Cell in the Frame

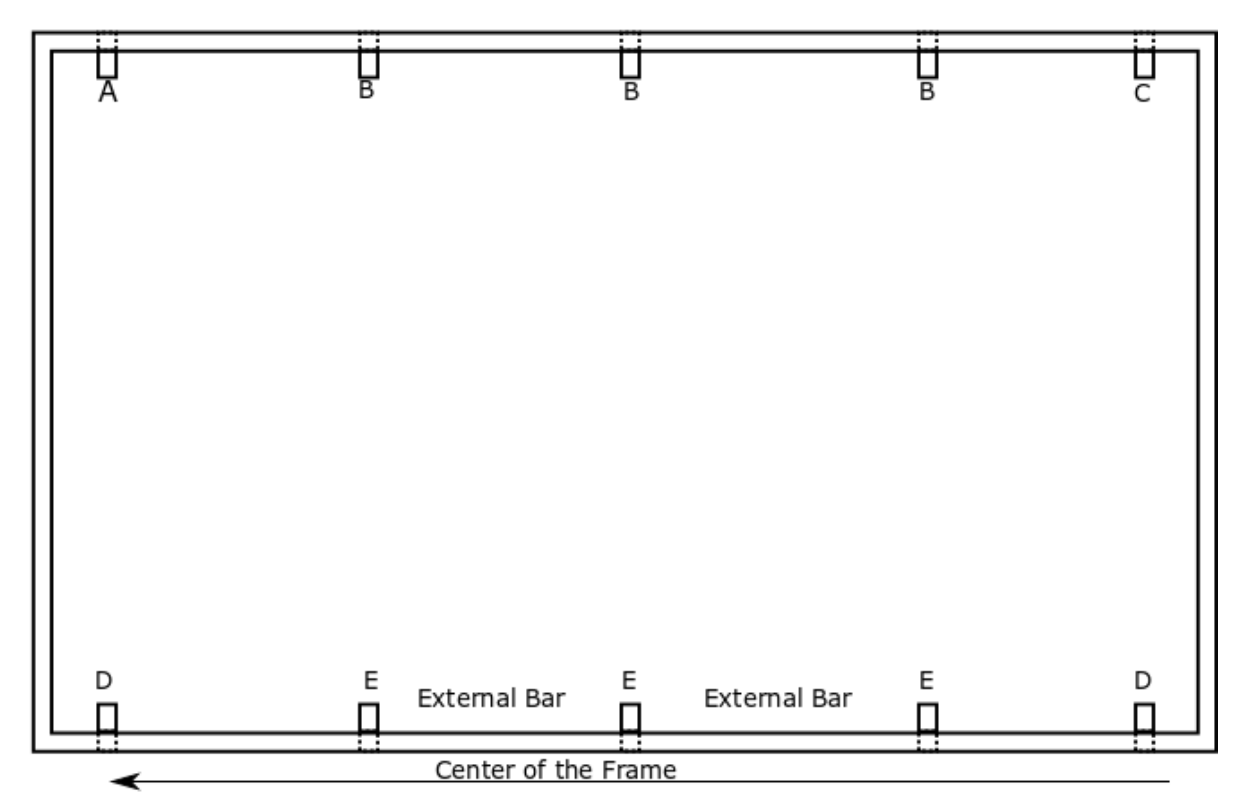


Figure 2.9. Garolite Inside a Border Cell in the Frame

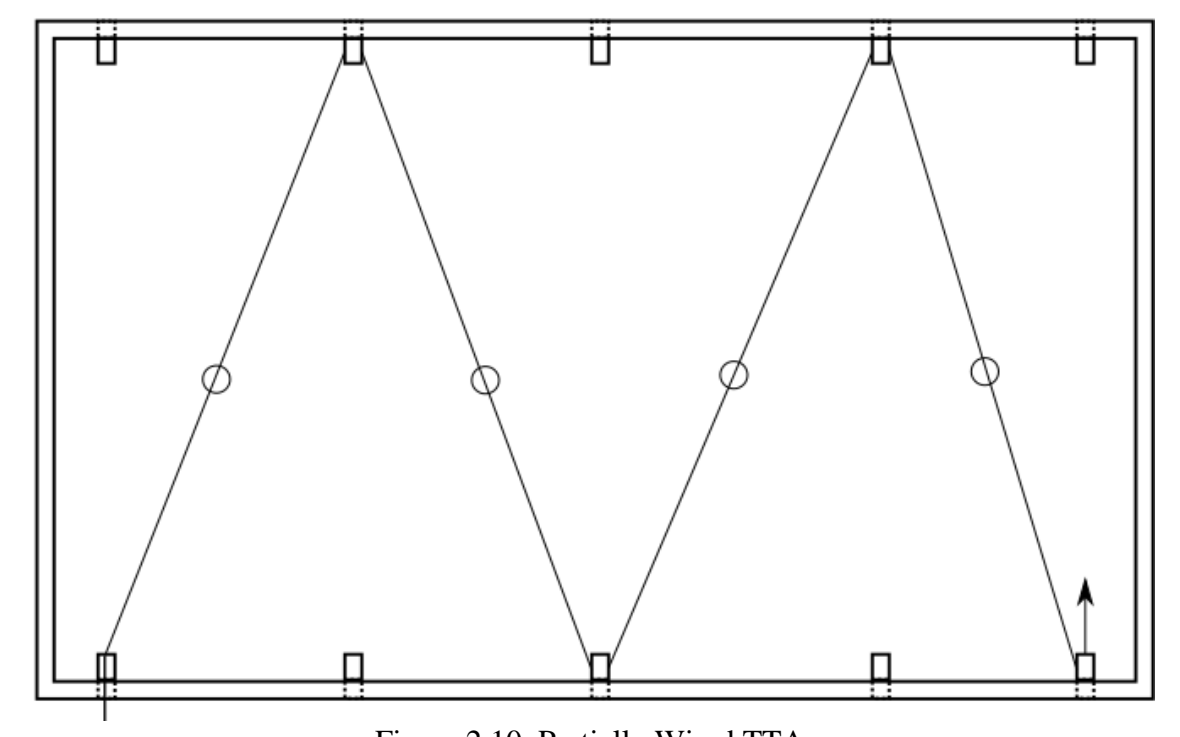


Figure 2.10. Partially Wired TTA

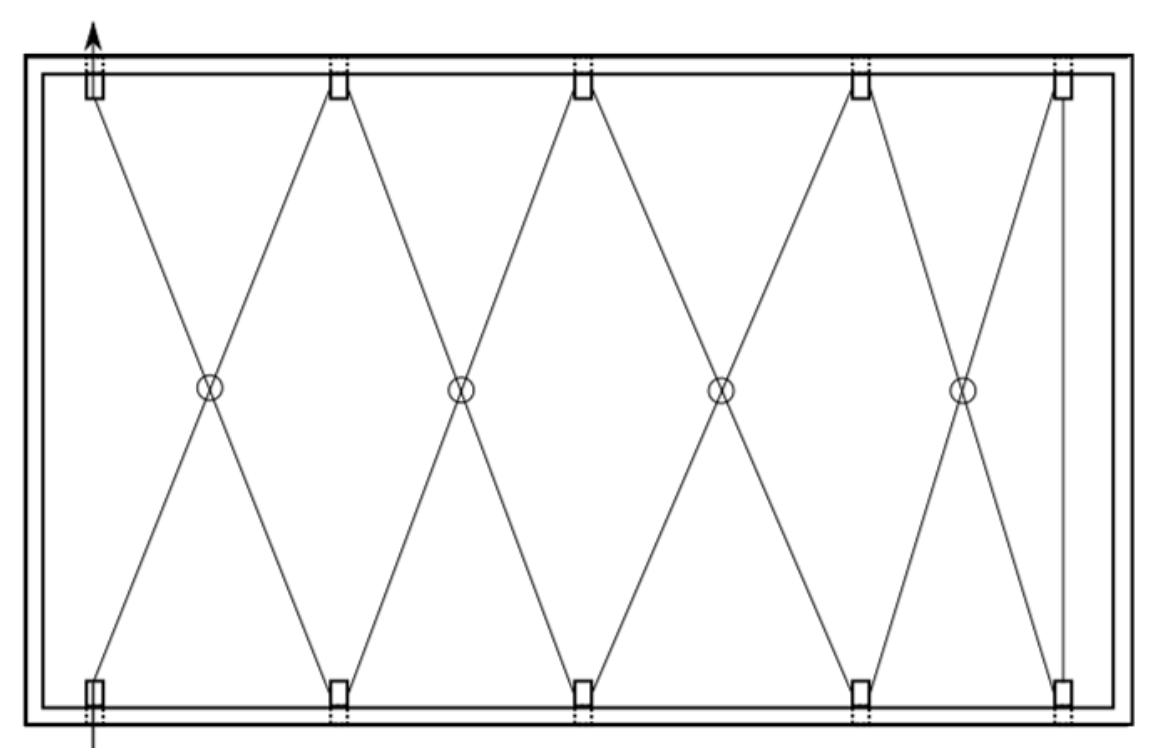


Figure 2.11. Fully Wired TTA

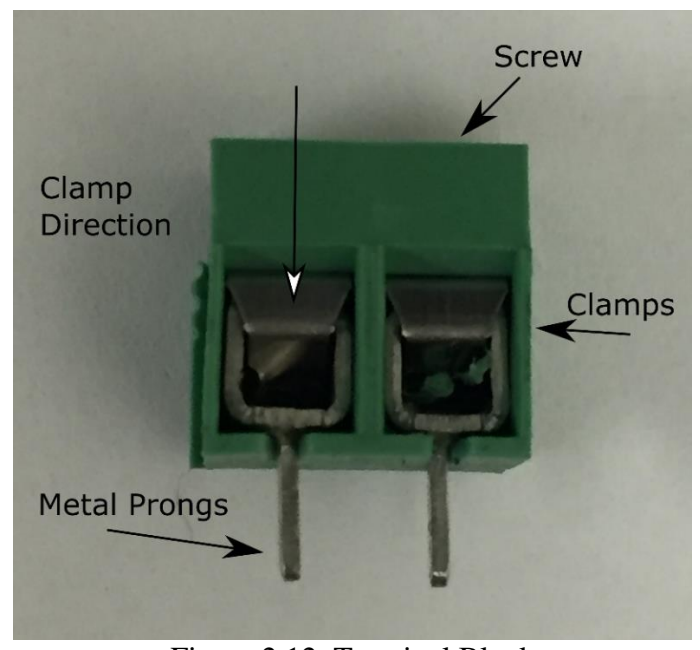


Figure 2.12. Terminal Block

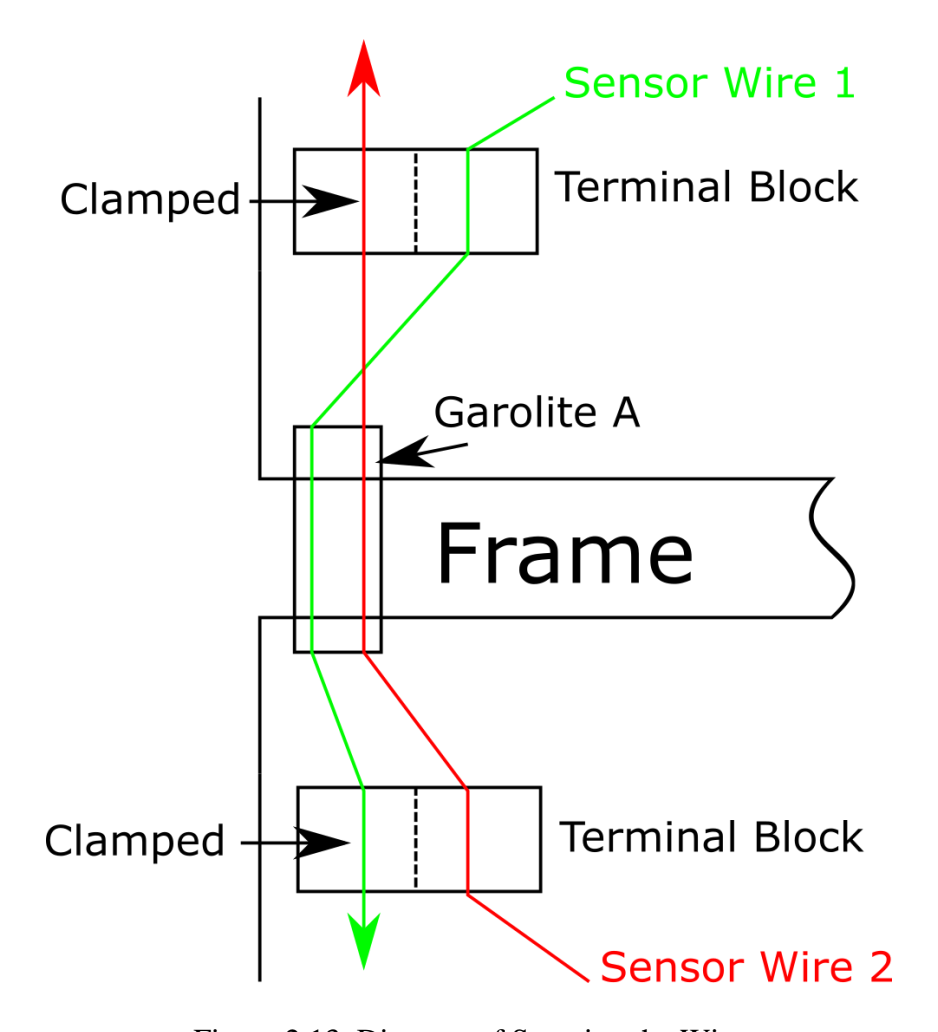


Figure 2.13. Diagram of Securing the Wire

## 2.3 Sensing Wire Characteristics

Tungsten wire was selected to be the sensing wire for the TTA given its high temperature coefficient of resistance. This allows the sensing wire has a linear correlation between temperature and electrical resistance.

$$R(T) = R_0 \left[ 1 + \zeta \left( T_w - T_{ref} \right) \right] \tag{3}$$

The TTA does not have a direct method of measuring the temperature of the sensing wire so with the temperature coefficient of resistance the temperature was calculated from the resistance of the wire. Since the wire was divided into segments, which will be discussed further in Section 3.1, the total wire resistance can be determined from the resistivity of the wire segments which are changing throughout the wire.

$$R(t) = \int_0^L \frac{\gamma(x,t)dx}{A_c} \tag{4}$$

The resistivity of the wire has a similar linear correlation to temperature as resistance which results in

$$\gamma(x,t) = 5.65 * 10^{-8} [1 + 4.5 * 10^{-3} (T_w(x,t) - 20)]$$
 (5)

The wire diameter was chosen to be 0.2 mm. If the wire was thicker diameter was chosen, the initial resistance would be lower and the TTA would have difficulty reading. If a thinner wire was selected, it was found that during the fabrication the wire would often break as a result of its small diameter.

The other factor that was affected by the wire temperature is thermal conductivity of the wire which increases with temperature, shown below. The temperature dependent expression for thermal conductivity is determined by fitting a third order polynomial to values reported in Fundamentals of Heat and Mass Transfer by Incorpra and DeWitt (2007) [8].

$$k(x,t) = -3.152 * 10^{-8} T_w(x,t)^3 + 1.128 * 10^{-4} T_w(x,t)^2 - 1.458$$

$$* 10^{-1} T_w(x,t) + 1.738 * 10^2$$
(6)

#### 3.0 Numerical Simulation of TTA Thermal Effects

### 3.1 Equation Derivation

The energy budget of a small segment of wire can be represented as shown in Figure 3.1.

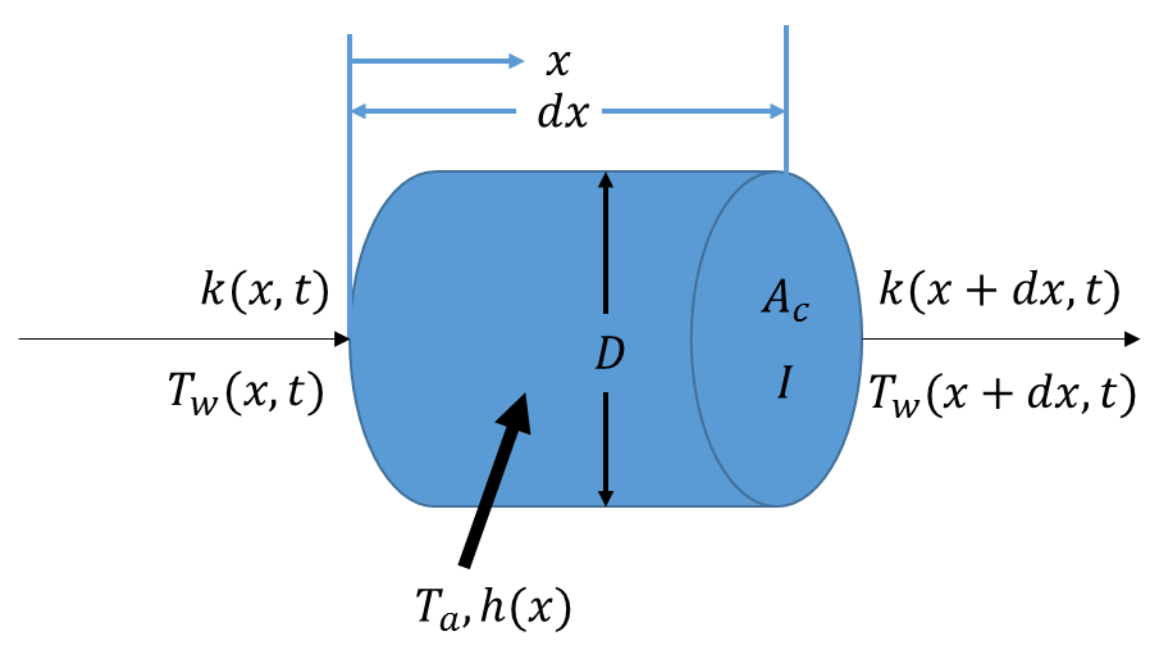


Figure 3.1. Energy Budget for a Wire Segment

The relationship between air speed and the rate of resistance-decay was simulated using the energy balance shown in Equation 7.

$$\dot{q}_{conduction} - \dot{q}_{convection} + \dot{q}_{generated} = \dot{q}_{stored} \tag{7}$$

Several assumptions were then considered. First, a one-dimensional heat transfer was considered due to the wire's small diameter and low Biot Number. Namely, the present Biot Number does not exceed 0.0003, whereas the condition to established 1D heat transfer is a Biot number less than 0.1. The heat stored in the wire causes the wire to change in temperature over time as expressed in Equation 8. The main source of heat leaving the system would be through heat convection which can be seen in Equation 9.

$$\dot{q}_{stored} = \rho C_p A_c \frac{\partial T_w(x, t)}{\partial t} dx \tag{8}$$

$$\dot{q}_{convection} = h(x, t)\pi D(T_w(x, t) - T_a)dx \tag{9}$$

The heat generated in the wire segment was caused by electrical current as expressed in Equation 10. Referring to Section 2.3, the resistivity of the wire, which increased due to temperature, is use due to the wire separated into segments.

$$\dot{q}_{generated} = I^2 dR(x, t) \tag{10}$$

$$dR(x,t) = \frac{\gamma(x,t)dx}{A_c} \tag{11}$$

$$\dot{q}_{generated} = I^2 \frac{\gamma(x,t)dx}{A_c} \tag{12}$$

As shown in Figure 3.1, axial conduction effects are included in the energy budget.

$$\dot{q}_{conduction} = -k(x,t)A_c \frac{\partial T_w(x,t)}{\partial x} + \frac{\partial}{\partial x} \left[ -k(x,t)A_c \frac{\partial T_w(x,t)}{\partial x} \right] dx \tag{13}$$

$$\frac{\partial}{\partial x} \left[ -k(x,t) A_c \frac{\partial T_w(x,t)}{\partial x} \right] dx = -A_c \frac{\partial}{\partial x} \left[ k(x,t) \frac{\partial T_w(x,t)}{\partial x} \right] dx$$

$$= -A_c \left[ \frac{\partial k(x,t)}{\partial x} \frac{\partial T_w(x,t)}{\partial x} + k(x,t) \frac{\partial^2 T_w(x,t)}{\partial x^2} \right] dx$$
 (14)

The equations above were inserted into Equation 7 to produce Equation 15. Equation 15 was then simplified to the form shown in Equation 16.

$$-k(x,t)A_{c}\frac{\partial T_{w}(x,t)}{\partial x}$$

$$-\left\{-k(x,t)A_{c}\frac{\partial T_{w}(x,t)}{\partial x} + \frac{\partial}{\partial x}\left[-k(x,t)A_{c}\frac{\partial T_{w}(x,t)}{\partial x}\right]dx\right\}$$

$$+h(x)\pi D(T_{w}(x,t) - T_{a})dx + I^{2}\frac{\gamma(x,t)dx}{A_{c}} = \rho C_{p}A_{c}\frac{\partial T_{w}(x,t)}{\partial t}dx$$

$$(15)$$

$$\frac{1}{\rho C_p} \frac{\partial k(x,t)}{\partial x} \frac{\partial T_w(x,t)}{\partial x} + \frac{k(x,t)}{\rho C_p} \frac{\partial^2 T_w(x,t)}{\partial x^2} - \frac{4h(x,t)}{\rho C_p D} (T_w(x,t) - T_a)$$

$$+ 16 \frac{I^2 \gamma(x,t)}{\rho C_p \pi^2 D^4} = \frac{\partial T_w(x,t)}{\partial t}$$
(16)

#### 3.2 Heat Convection

The heat transfer coefficient (h) depends on the Nusselt Number as expressed in Equation 17.

Various Nusselt Number correlations were considered for the simulation:

- i. Hilpert (1933)
- ii. Fand and Keswani (1961)
- iii. Zukaukas (1987)
- iv. Churchill and Burnstein (1977)
- v. Morgan (1975).

These correlations were found in <u>Natural Convection from Circular Cylinders</u> [1]. The selected correlation was established by Bruun (1995) [2] which can be seen in Equation 18.

$$h(x,t) = k_a \frac{Nu}{L} \tag{17}$$

$$Nu = 0.981Re^{0.33}Pr^{1/3} (18)$$

This correlation was created for hot-wire anemometry, which in this correlation and experiment uses a thin wire. It was also determined that using Brunn resulted in the smallest deviation between the simulation and the experimental results, which will be later discussed in Section 4.3

Various properties of air were reliant on the wire temperature as represented by the film temperature. See Equation 19. The Reynolds Number and the Prandlt Number which are dependent upon the film temperature as defined in Equation 20, 21, and 22. The information in Equation 21

and 22 was obtained from an extrapolation from the <u>Fundamentals of Heat and Mass Transfer</u> by Incorpra and DeWitt (2007) [8].

$$T_{film}(x,t) = \frac{T_w(x,t) + T_a}{2}$$
 (19)

$$Re(x,t) = \frac{U(x)D}{v_{film}(x,t)}$$
(20)

$$v_{film}(x,t) = 3.88 * 10^{-17} T_{film}(x,t)^{5} + 5.70 * 10^{-15} T_{film}(x,t)^{4} - 3.94$$

$$* 10^{-13} T_{film}(x,t)^{3} + 1.69 * 10^{-15} T_{film}(x,t)^{2} - 1.93 * T_{film}(x,t)$$

$$+ 1.01 * 10^{-5}$$
(21)

$$Pr(x,t) = 6.36 * 10^{-14} T_{film}(x,t)^{5} + 1.56 * 10^{-11} T_{film}(x,t)^{4} - 2.90$$

$$* 10^{-9} T_{film}(x,t)^{3} + 9.67 * 10^{-7} T_{film}(x,t)^{2} - 2.28$$

$$* 10^{-4} T_{film}(x,t) + 7.20 * 10^{-1}$$
(22)

#### 3.3 Boundary Conditions

An adiabatic boundary condition was assumed for the wire:

$$\frac{\partial T(0,t)}{\partial x} = 0 \tag{23}$$

$$\frac{\partial T(L,t)}{\partial x} = 0 \tag{24}$$

This was due to the material holding the wire having thermally nonconductive material holding the wire as stated in Section 2.2.

#### 3.4 Simulation

The simulation used a forward marching scheme in space and time. For the end segments the simulation used first order difference, due to the end segments being adiabatic. Whereas the other segments used second order central difference. The dx used for this problem was 1mm and

the dt was 0.001 seconds due to the stability criteria. A smaller value for dx would require the dt to be divided by the square of the dx's incremental decrease to keep stability causing the computational time to increase drastically. The simulation was set to end when a non-dimensional resistance reaches exp(-1).

#### 3.5 Verification

The verification process will be carried out in two steps. Step one evaluates the cooling of the wire. A simplified problem was tested to verify cooling of the wire. More lenient assumptions and conditions were introduced for the numerical solution. This verification solution applies to the time period after the heating of the wire. Some assumptions include; uniform air flow (removes the axial conduction and the need to separate the wire into segments), the terms in the heat convection are at ambient air conditions (rather than the changing film temperature) and the removal of the energy generation (the energy generation was due to the small sense current that was used to determine R(t) but in this study its contribution was negligible), see Equation 25 for the simplified equation. This produces an exponential decay which was expected from the previous work (Section 1.2). The exponential decay is shown in Figure 3.2.

$$-h\pi DL(T(t) - T_a) = \rho C_p A_c L \frac{dT}{dt}$$
(25)

$$(T(t=0) - T_a) \exp\left(-\frac{4h}{\rho C_p D}t\right) + T_a = T(t)$$
(26)

$$\Theta = \frac{T_w(x,t) - T_a}{T(x,t=0) - T_a} = \frac{R(t) - R_a}{R(t=0) - R_a}$$
(27)

# Exponential Decay of Uniform Velocity Profile (Average Air Speed = 10 m/s)

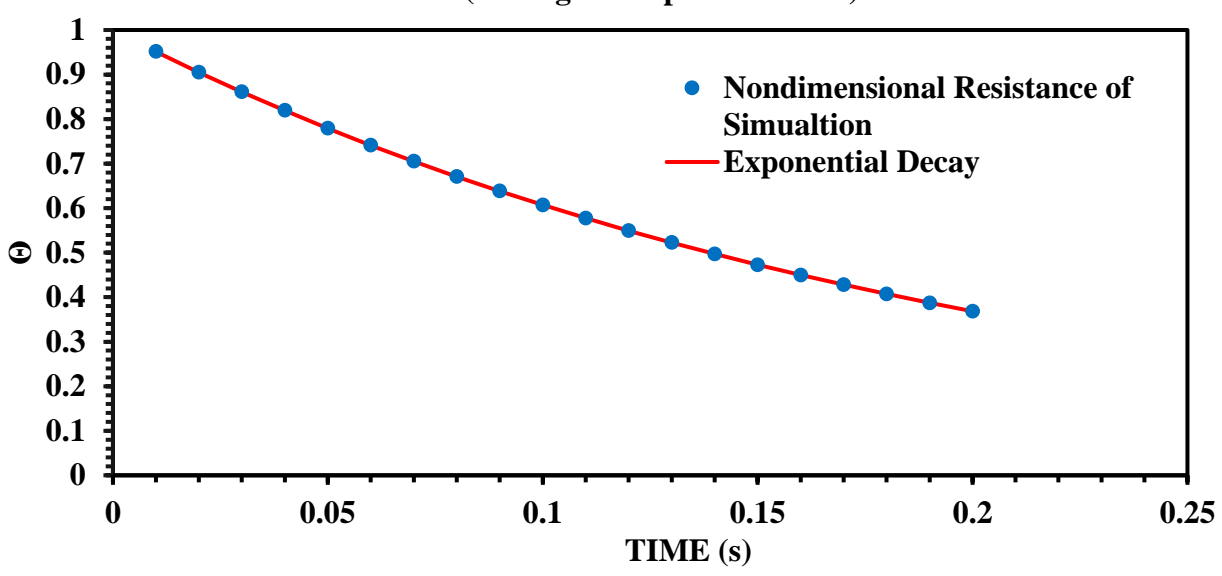


Figure 3.2. Comparing Exponential Decay to Experimental Nondimensional Resistance

Step two evaluates the axial conduction of the wire. To verify the effects of the axial conduction was implemented correctly Equation 16 was solved numerically for the heating of the wire. Several simplifications were made to Equation 16 which were assuming thermal conductivity and heat convection were constant. To create a need for axial conduction an initial temperature of the wire was imposed. This process of reaching a numerical solution used separation of variables, which can be found in Conduction of Heat in Solids [3] and Heat Conduction [4]. The two initial conditions tested for the wire is expressed in Equations 28 and 29. This produces Equations 30 and 31, which are derived in Appendix C. The two methods were then plotted against each other using a 10 m/s air speed and a current of 2 Amps as inputs.

$$T_{w,linear}(x,t=0) = \frac{20x}{L} + T_a$$
 (28)

$$T_{wire,parabolic}(x, t = 0) = -40x^2 + 40x + T_a$$
 (29)

$$T_{w,linear}(x,t) = -\frac{a}{v}$$

$$+ \sum_{n=1}^{\infty} \left[ \frac{40(\cos(n\pi) - 1)}{n^2 \pi^2} + 10 + T_a \right]$$

$$+ \frac{a}{v} \cos\left(\frac{n\pi x}{L}\right) \exp(-(\alpha \lambda^2 - v)t)$$
(30)

 $T_{w,parabolic}(x,t) =$ 

$$-\frac{a}{\nu} + \sum_{n=1}^{\infty} \left[ \frac{-80(\cos(n\pi) + 1)}{n^2 \pi^2} - \frac{40L}{3} + 20 + T_a + \frac{a}{\nu} \right] \cos\left(\frac{n\pi x}{L}\right) \exp(-(\alpha \lambda^2 - \nu)t)$$
(31)

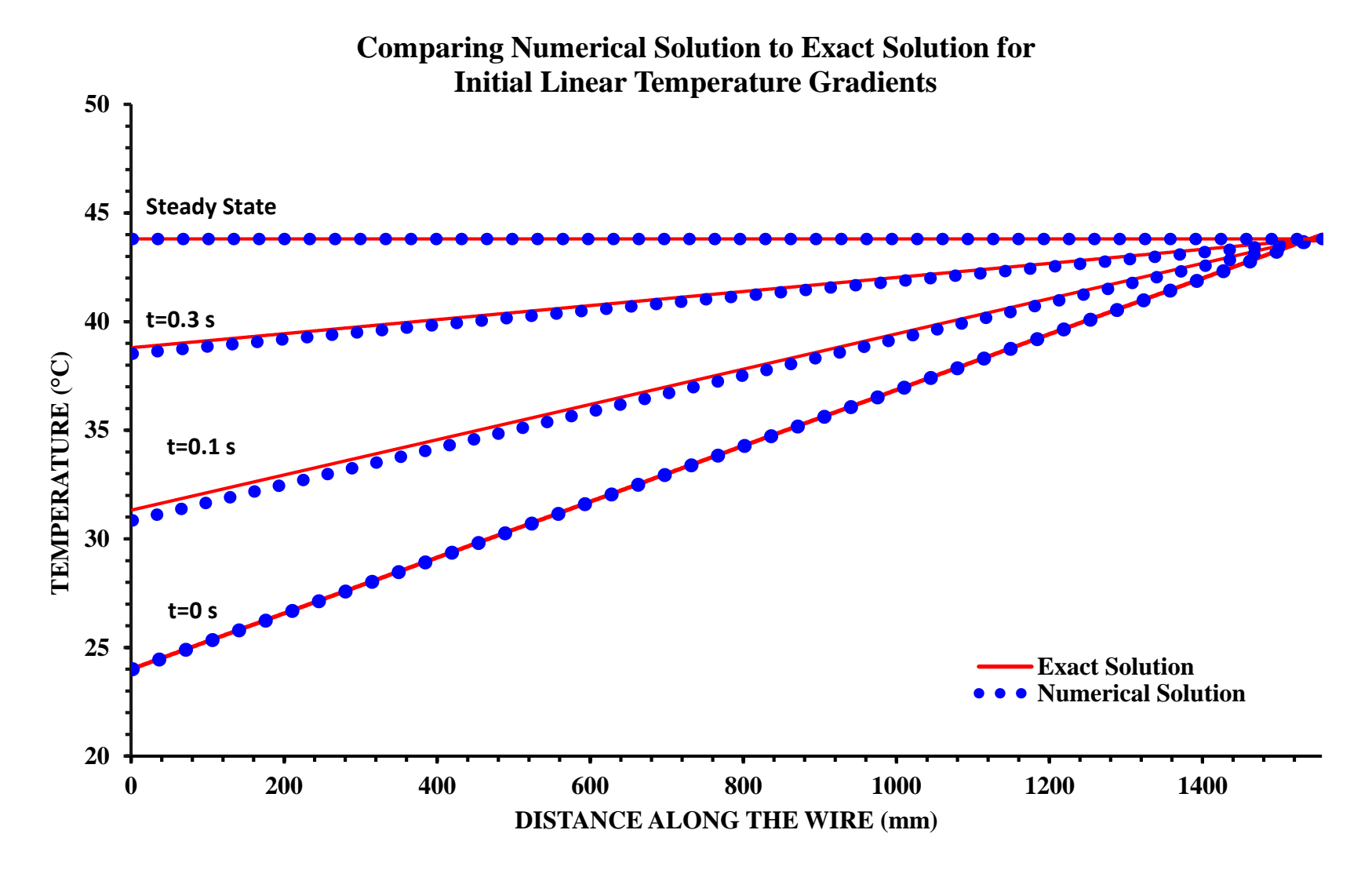


Figure 3.3. Comparing Numerical Solution to Exact Solution for a Wire with an Initial Linear Temperature Profile

# Comparing Numerical Solution to Exact Solution for Initial Parabolic Temperature Gradients

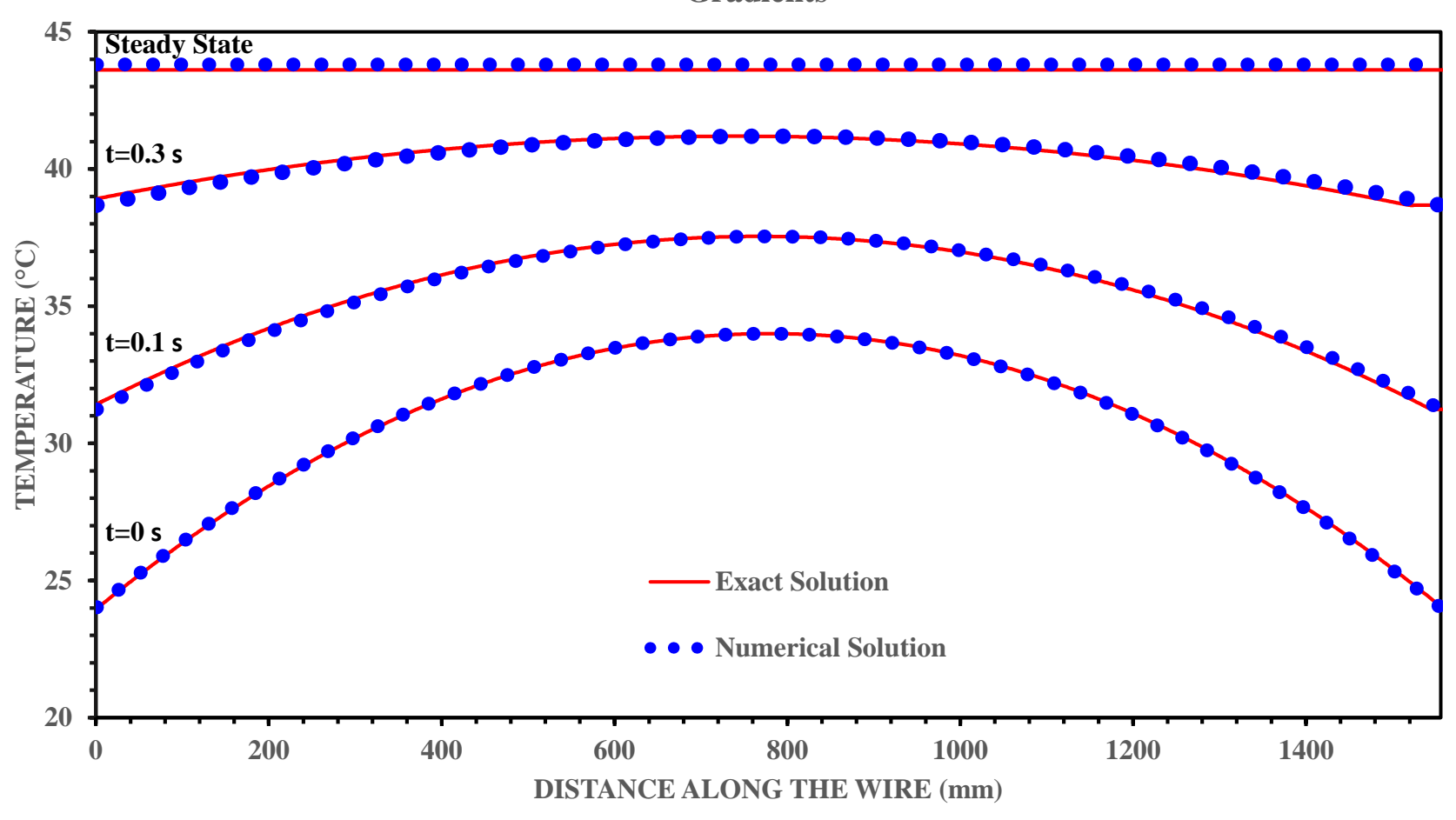


Figure 3.4. Comparing Numerical Solution to Exact Solution for a Wire with an Initial Parabolic Temperature Profile

### 4.0 Experimental Investigation

## **4.1 Test Facility**

The test facility was designed to obtain data from the TTA as shown in Figure 4.1. The test facility used a Buffalo Forge Blower to create an air flow over the frame. Note that a contraction exists in the facility between the TTA and the blower; see Figure 4.2. Figure 4.3 shows the TTA frame mounted at the facility entrance. Shown on the front view of the facility is the TTA held in place during testing. Cardboard cylinders were cut in half and placed around the perimeter of the opening on the plywood, which creates a bell mouth entrance. Another front view can be seen in Figure 4.4, where a plastic honeycomb (a flow straightener) was placed at the front of the TTA to ensure that the flow was homogenously perpendicular to the TTA. The blower motor was not adjustable; hence, to change the air speed over the face of the TTA, the facility utilized a controlled air bleed as shown in Figure 4.1. This was accomplished with a sliding door on the side of the facility (Figure 4.5 and 4.6) and by removing the plates on the top and the bottom to increase the bleed and reduce the airflow over the TTA. This reduced the volume air flow from the front of the facility. When the airspeed was required to increase, ridged plastic sheets were used to block the upper or lower two rows of the frame. When the top three rows were tested, the fifth and sixth row were blocked. When the bottom three rows were tested, the first and second rows were blocked. Later when testing the radiator, the radiator was supported behind the plywood (with several brackets). The TTA was attached behind the radiator and the shroud was placed behind the radiator as shown in Figure 4.8.



Figure 4.1. Side View of TTA Testing Facility



Figure 4.2. Front View of TTA Testing Facility

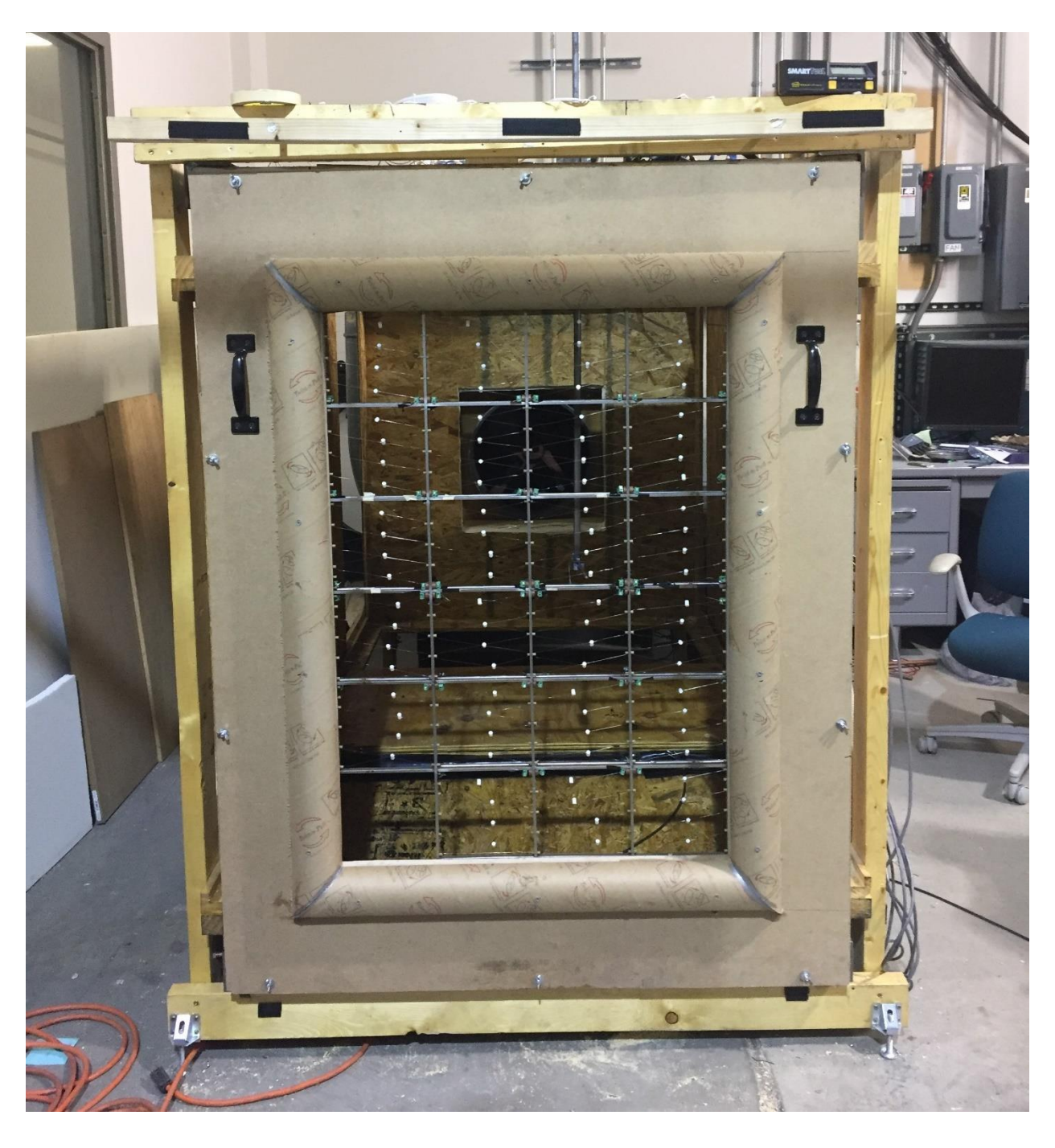


Figure 4.3. TTA Testing Facility with TTA Installed

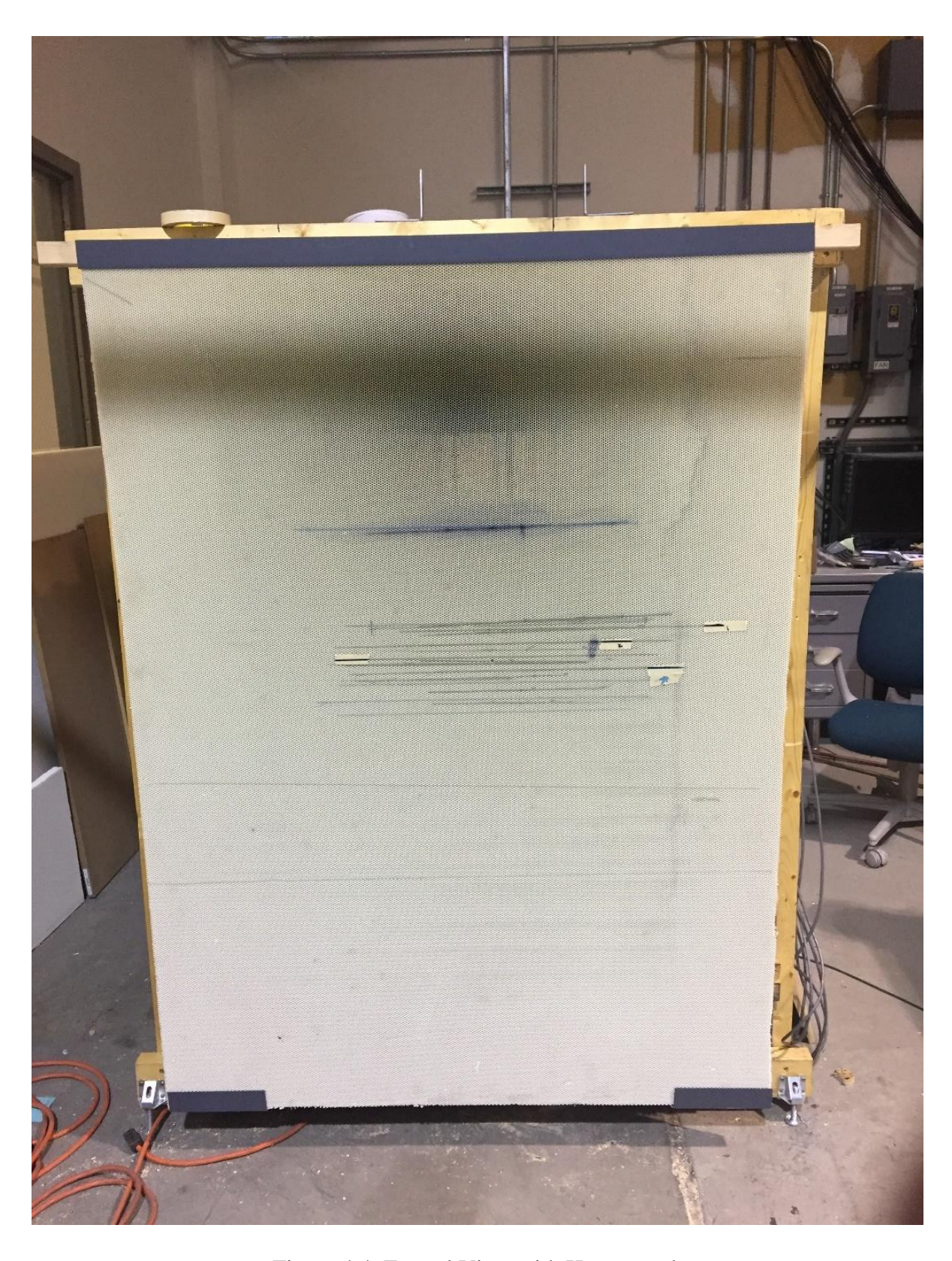


Figure 4.4. Frontal View with Honeycomb



Figure 4.5. TTA Testing Facility with No Air Bleed



Figure 4.6. TTA Testing Facility with Large Amount of Bleed



Figure 4.7. View of Testing Facility with Radiator Installed

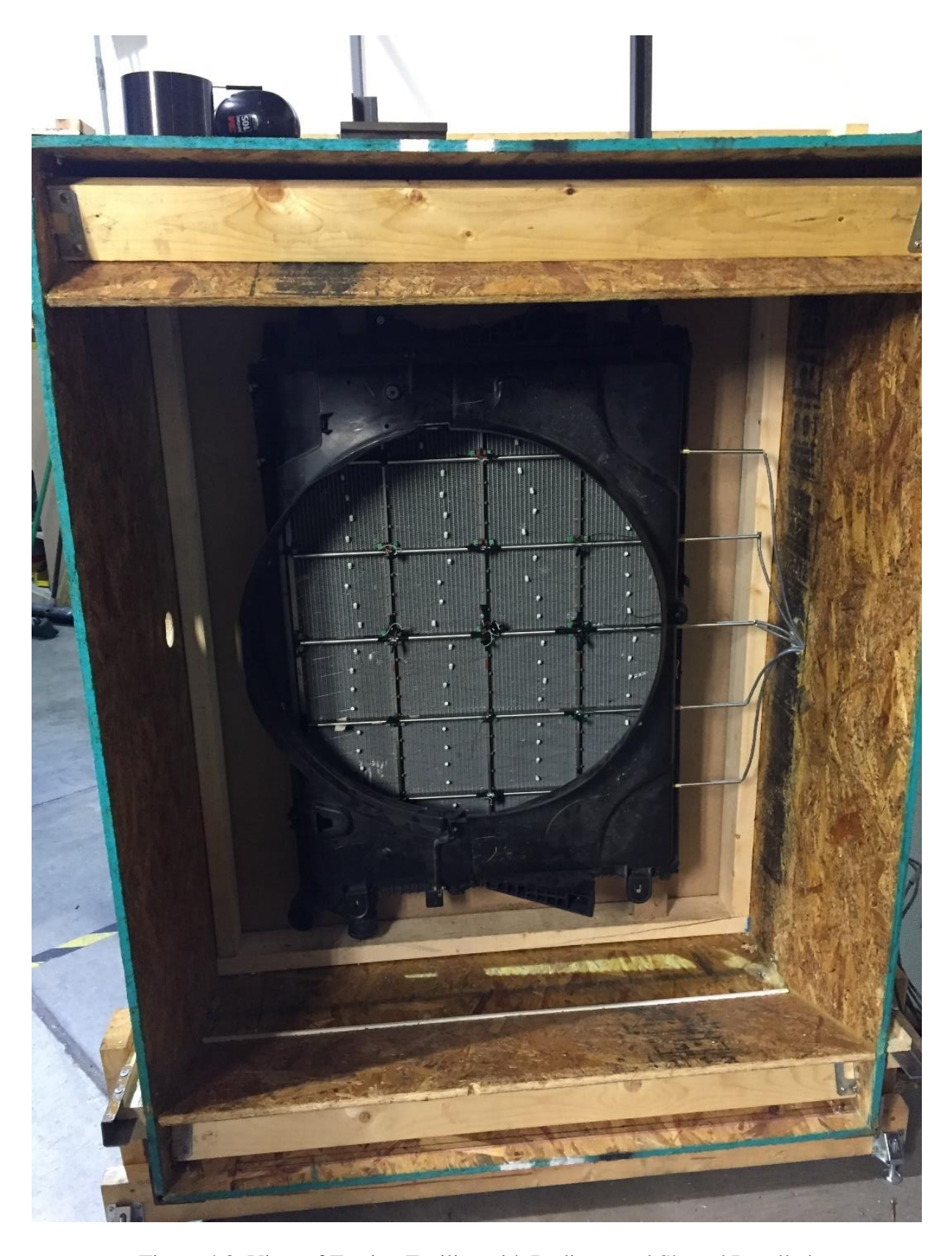


Figure 4.8. View of Testing Facility with Radiator and Shroud Installed

### **4.2 Hot-Wire Probe Anemometry**

A Disa 55M Constant Temperature Anemometer (CTA) was used to define the velocity magnitudes in this study. The associated hot wire probe is shown in Figure 4.9. The two prongs hold a plates 5-micron tungsten wire that is maintained at an elevated constant temperature. The CTA measures air speed by interpreting the magnitude of the input power that is required to maintain a constant resistance of the 5-micron wire.



Figure 4.9. Image of the Hot Wire Probe



Figure 4.10. Image of the Hot Wire Probe Close Up

### **4.3 CTA Calibration**

The hot-wire probe was placed in a calibration facility as shown in Figure 4.11. The facilities' blower provided a known air flow at the hot wire probe. The plenum pressure  $(P_{p1})$  can be utilized directly for the upper range ( $\geq 4$  m/s) velocity values (U) at the vena contracta of the slit jet (x/w $\approx 1.5$ ). Appendix A describes the unique procedure to resolve the measurement uses associated in the lower range velocity values. Blockage was placed over the blower to get various

speeds of air over the probe. Data was taken over a one-minute interval. The hot wire probe was connected to the Sakor Unit which collected the voltage used to keep a constant temperature. The data was averaged over the one-minute interval and was compared to the air speed of the air. This created a relationship between the voltage (E) to maintain a constant temperature of the hot-wire probe see Figure 4.12.

$$E^2 = A + BU^{0.43} (32)$$



Figure 4.11. Hot Wire Probe Calibration Facility

### **Probe Calibration**

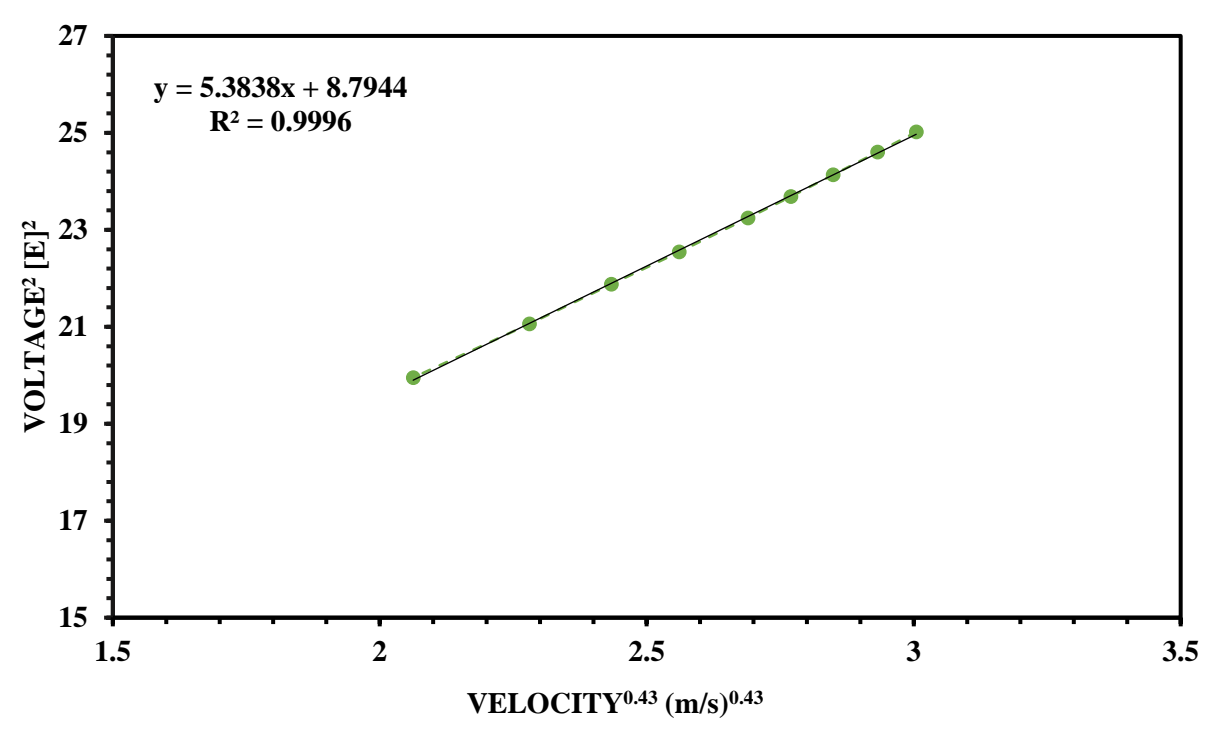


Figure 4.12. Hot Wire Probe Calibration

### **4.4 TTA Frame Calibration**

The TTA frame was placed in the TTA test facility. The hot-wire probe was clamped to a rod that moved vertically. The CTA sensor was placed 5 cm behind the TTA frame at the third cell. This cell was selected because it was displaced from the walls of the facility and would experience the least effect from the side wall boundary layer. The probe was able to move from row to row with respect to the frame. Each cell was tested with a four-second test interval for four minutes. The Sakor unit creates a text file for each four-minute trial. Hence, with data handing overhead, each datum point in Figure 4.13 represents nominally 10 TTA samples. The calibration for the other rows can be viewed in Appendix B.

## **TTA Row 3 Calibration**

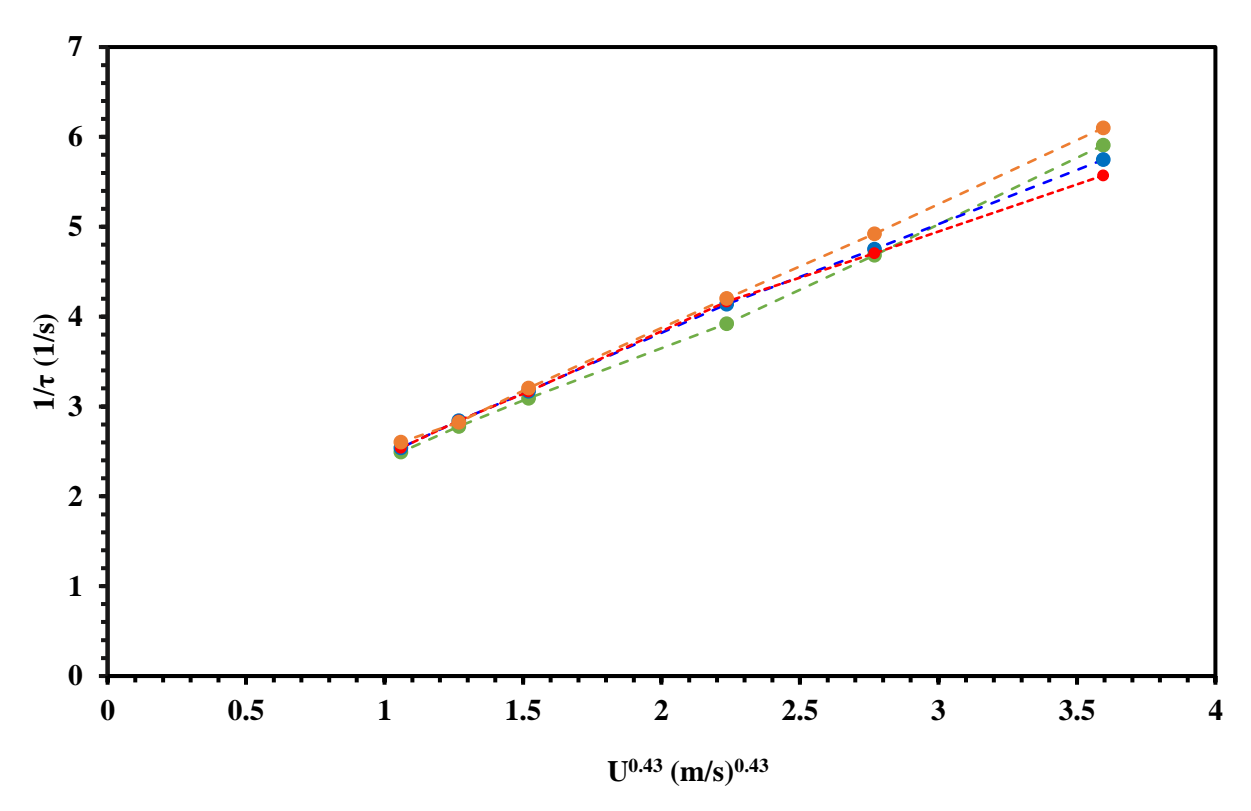


Figure 4.13. Example of a Row Calibration of the TTA Note,  $y_i$  (i=1, 2, 3, 4) represent the cell number for a given row.

### **5.0 Numerical Simulation Results Compared with Experiments**

Shown below is the comparison between the values of tau between the simulation to the TTA at the given air speed from the calibration. The values of  $\tau$  from the TTA system was typically greater than the values from the simulation. This demonstrates the effect of the Garolite and the Teflon spacers acting as heat sinks that was not taken to account in the simulation, which caused the simulation to become unstable.

$$\delta \tau = \frac{\tau_{measured} - \tau_{simulated}}{\tau_{measured}} \times 100\%$$
 (33)

### **Comparison of Row 1 to Simulation**

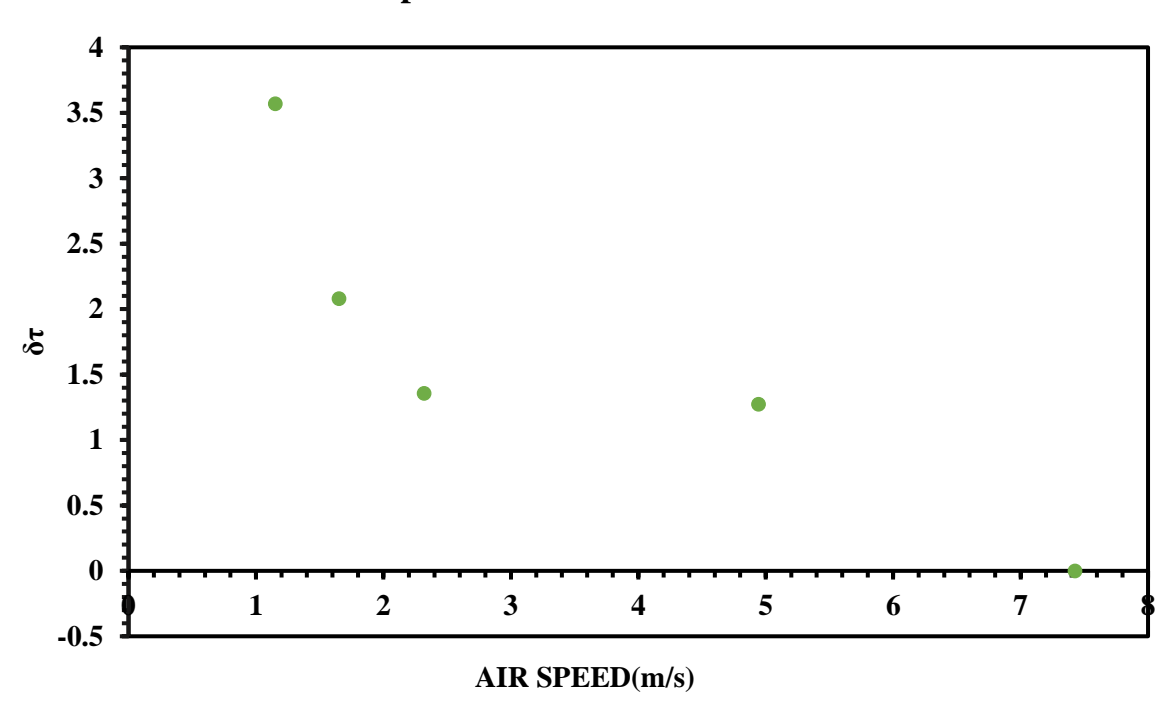


Figure 5.1. Comparison of  $\tau$  Between Row 1 to Simulation

## **Comparison of Row 2 to Simulation**

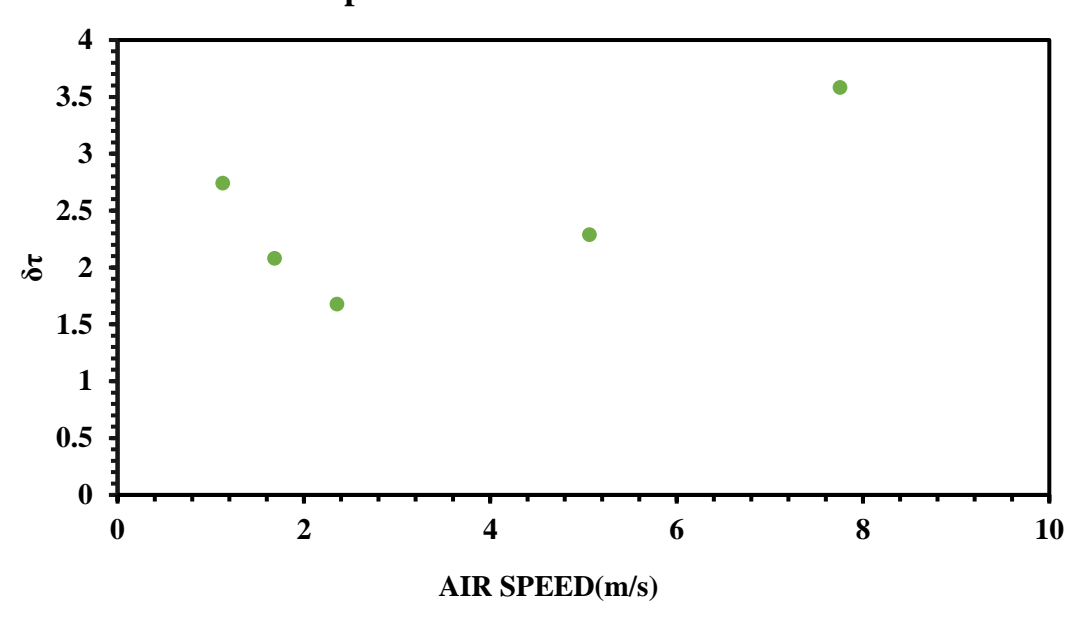


Figure 5.2. Comparison of  $\tau$  Between Row 2 to Simulation

## Comparison of Row 3 to Simulation

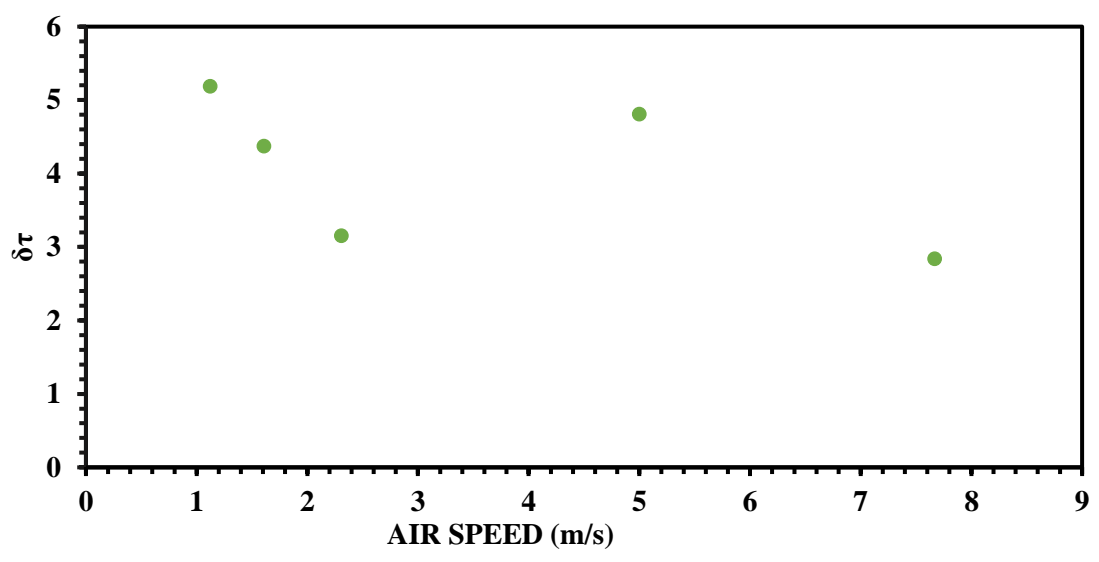


Figure 5.3. Comparison of  $\tau$  Between Row 3 to Simulation

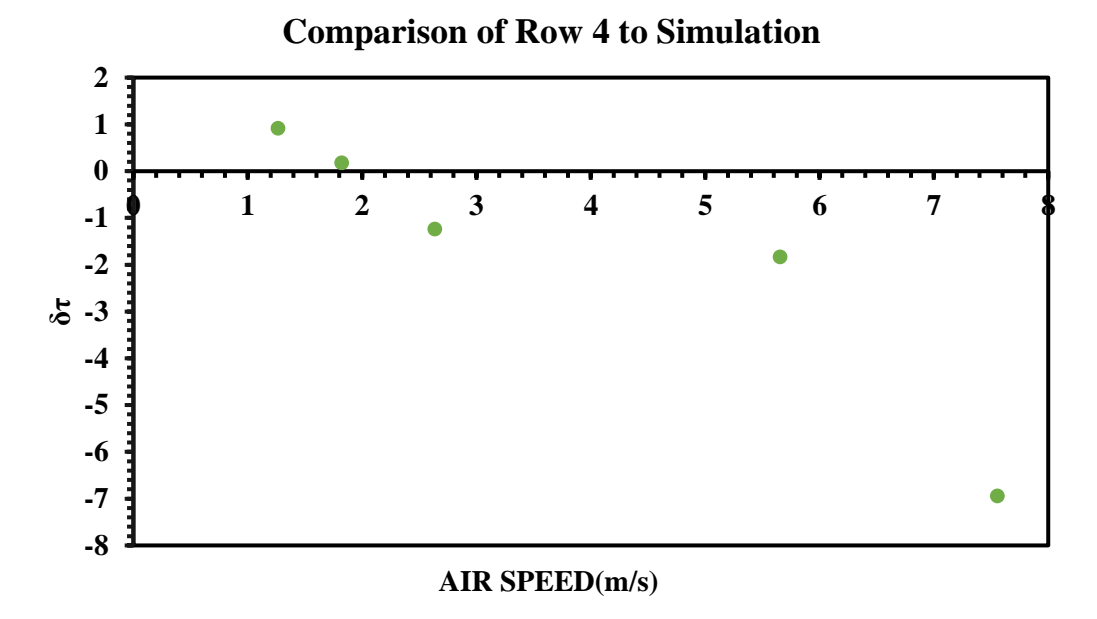


Figure 5.4. Comparison of  $\tau$  Between Row 4 to Simulation

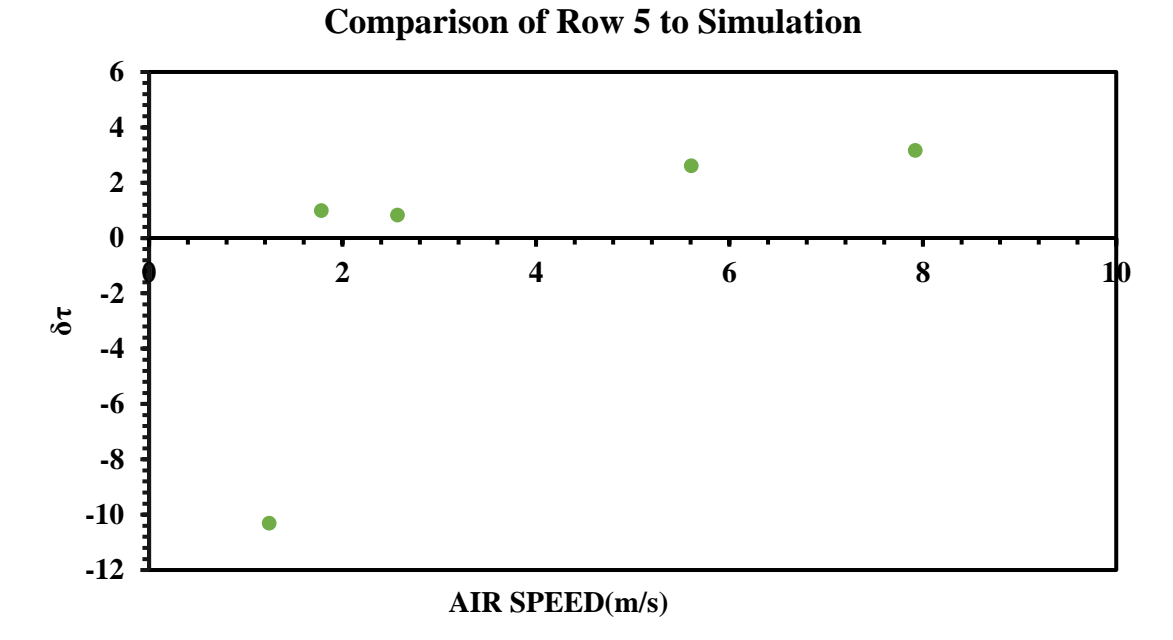


Figure 5.5. Comparison of  $\tau$  Between Row 5 to Simulation

# Comparison of Row 6 to Simulation

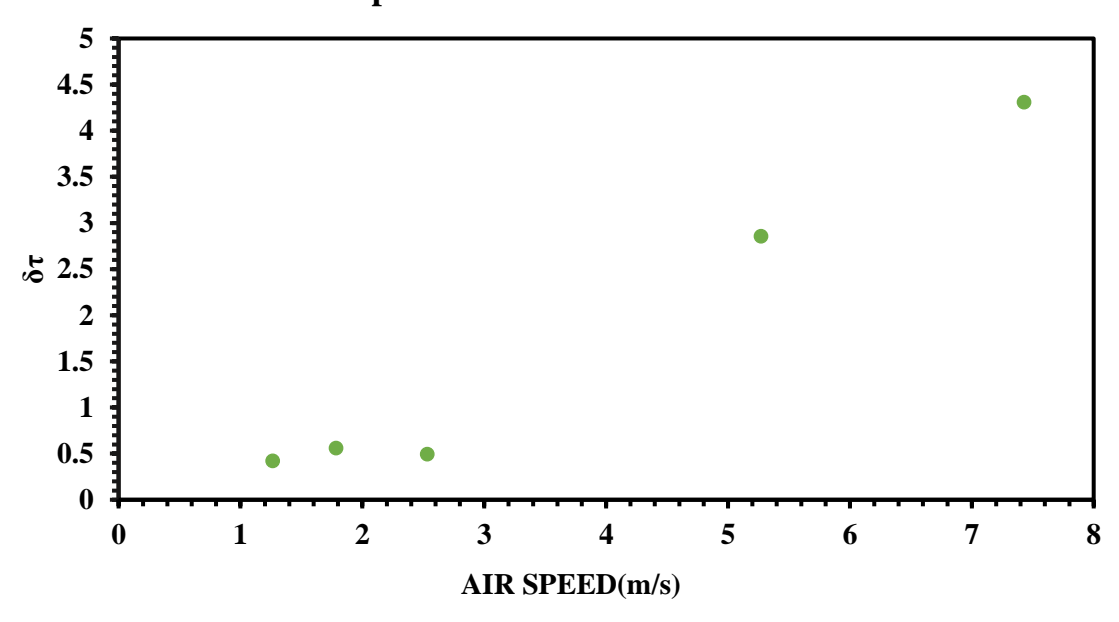


Figure 5.6. Comparison of  $\tau$  Between Row 6 to Simulation

### 6.0 Non-uniform Velocity Profile

### **6.1 Experimental Procedure for the Non-uniform Velocity Distribution**

The TTA was removed from the test facility and the probe was moved forward two inches at the equivalent third cell of the third row. Hence, the probe measured the air velocity at the plane of the sensing wires of the TTA. A cloth was wrapped around a wooden frame at with an increasing layer every 1/8 of an inch, beginning 3/16 of an inch from the bottom of the cell; see Figure 6.1. The result was to create a gradient in the air flow velocity field. Measurements were made for 1-minute intervals at each 1/8-inch interval of the cloth thickness. The probe was removed and the TTA frame was returned to the test facility. TTA data were then obtained in a 4-minute interval with samples collected every 4 seconds. These data were averaged over the four-minute interval.



Figure 6.1. TTA Testing Facility with Cloth Gradient Over the Face

### **6.2 Experimental Results**

The non-uniform flow that was present at the face with Row 3, Cell 3 (measured by the hot wire probe) is shown in Figure 6.2. The non-uniform flow produced a tau value of 0.254 seconds. This caused the TTA to consider the flow to be 4.55 m/s based on the calibration. This differs from the spatially averaged velocity: 5.35 m/s that has a percent difference of 15.0 % to what the TTA system to consider.

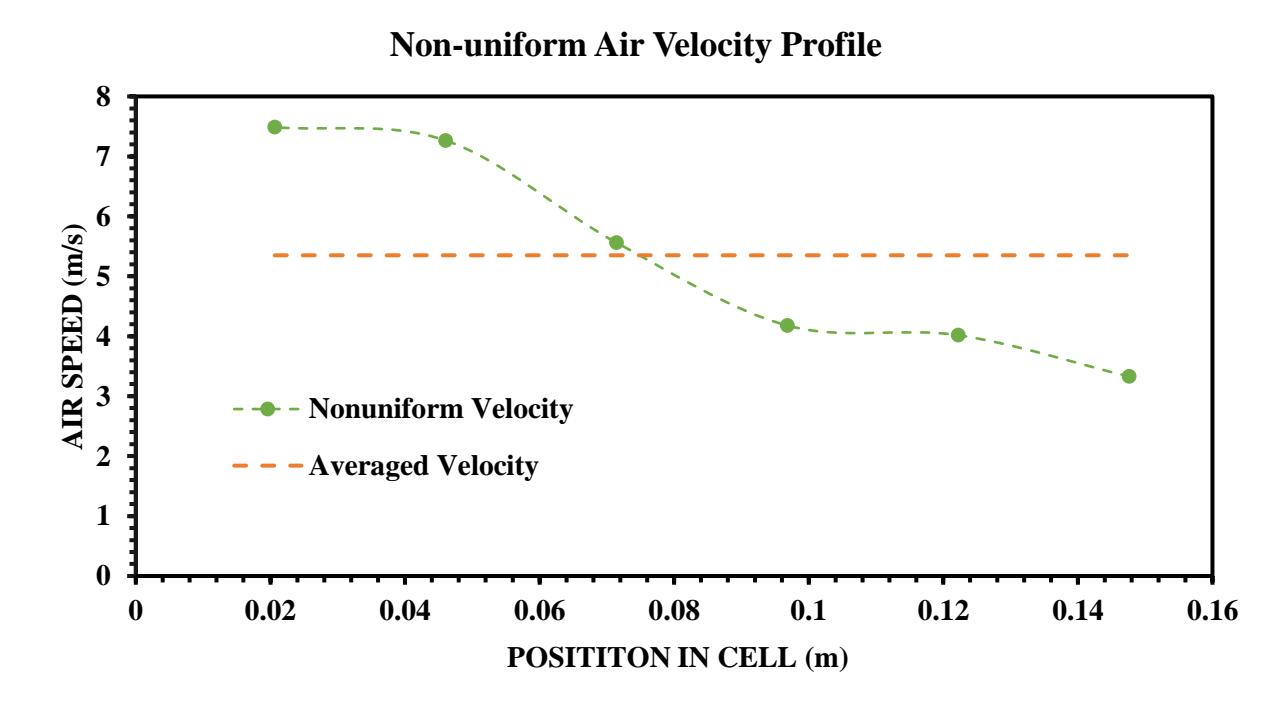


Figure 6.2. Non-uniform Flow Over Row 3, Cell 3 Measured with Hot-Wire Probe

### **6.3 Simulation Comparison**

The temperature decay in the TTA subjected to the velocity profile shown in Figure 6.2 was simulated. The temperature decay with the non-uniform flow form Equation 34 (which fit a fifth order polynomial over the data points of the points on Figure 6.2) as an input. When this equation was simulated, the resulting tau of 0.254 seconds matched the experimental data. Uniform flows were simulated over a large range to create a relationship between a uniform velocity and tau. Various non-uniform fluid flows were then tested and compared to what the TTA would

considers to be the uniform flows based on the tau to air velocity correlation done with uniform flow. As seen in this table various parameters caused the difference between a non-uniform flow and the perceived uniform flow, which will be discussed in Section 7.3.

$$U(x) = -1.3705 * 10^{6}x^{5} + 3.9852 * 10^{5}x^{4} - 2.5798 * 10^{4}x^{3} - 1.3767$$
$$* 10^{4}x^{2} + 1.1644 * 10^{2}x + 5.8295$$
 (34)

### 7.0 Simulations of Non-Uniform Velocity Profiles

### 7.1 Simulated Temperature Distribution for Non-Uniform Velocity

Various velocity profiles were inserted as input for the simulation of the temperature decay. Velocity profiles such as linear (Equation 35 and 36), parabolic (Equation 37), and sinusoidal (Equation 38) for example were tested with a straight wire (diameter of 0.2 mm, length of 1.556 meters).

$$U_{linear}(x) = 10\left(\frac{x}{L}\right) + 5\tag{35}$$

$$U_{linear}(x) = U_{avg} + \frac{b}{2}(2x - L) = 10 + \frac{10}{2}(2x + L)$$
 (36)

$$U_{parabolic}(x) = -40\left(\frac{x}{L}\right)^2 + 40\left(\frac{x}{L}\right) + 5 \tag{37}$$

$$U_{sinusoidal}(x) = \frac{5\sin\left(\frac{2\pi x}{L}\right)}{2} + 10 \tag{38}$$

The resulting temperature transient distributions are associated with these velocity fields are shown in Figures 7.2-7.4 (with Figure 7.1, a uniform velocity profile, as a comparison). Then the nondimensional resistance (or nondimensional average temperature) was compared to the exponential decay from Section 1.2. This is shown in Figures 7.5-7.7. The temperature decay follows the exponential decay, regardless of the different velocity distribution.

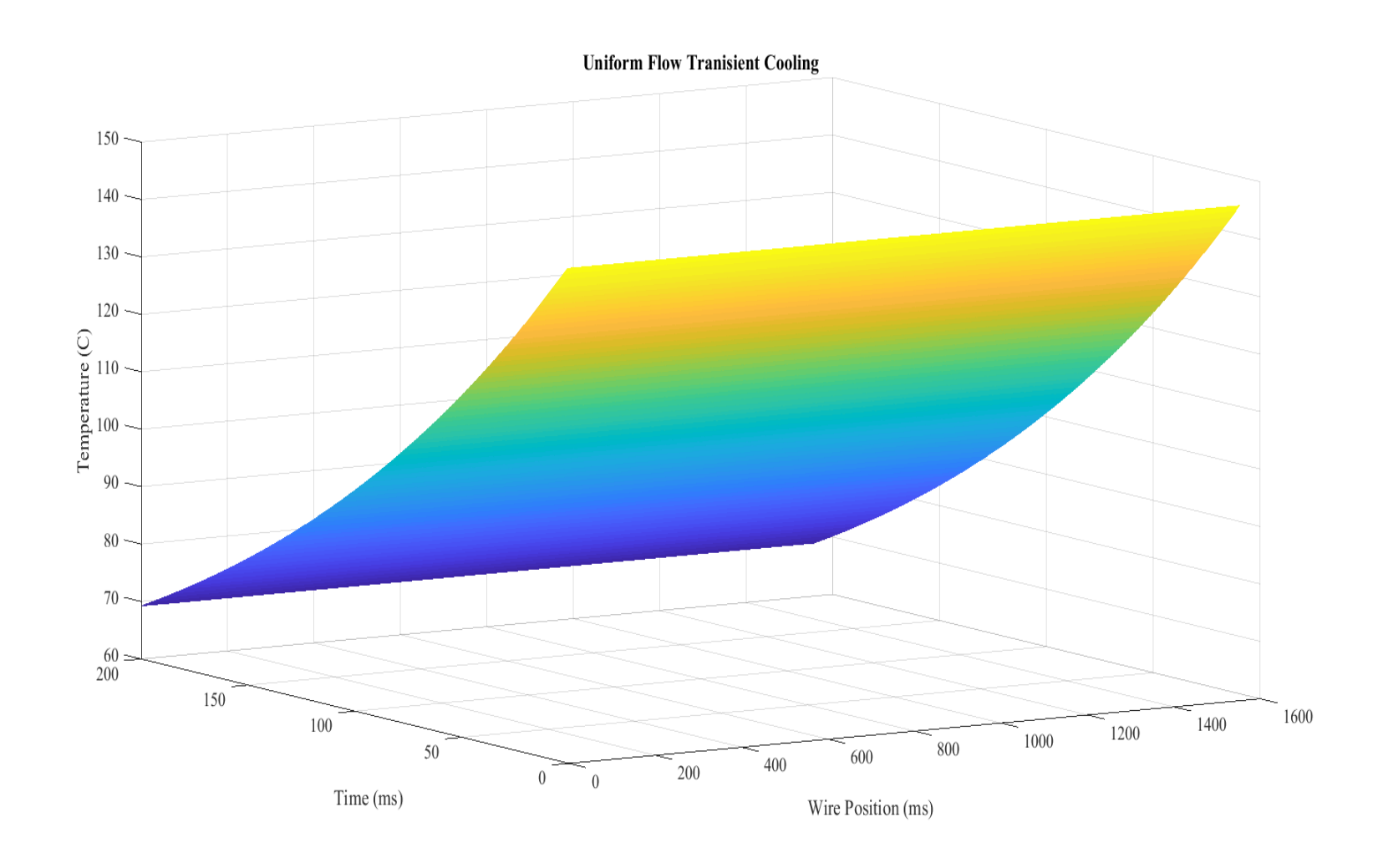


Figure 7.1. Transient Cooling Under Uniform Flow, Speed of  $10\ \text{m/s}$ 

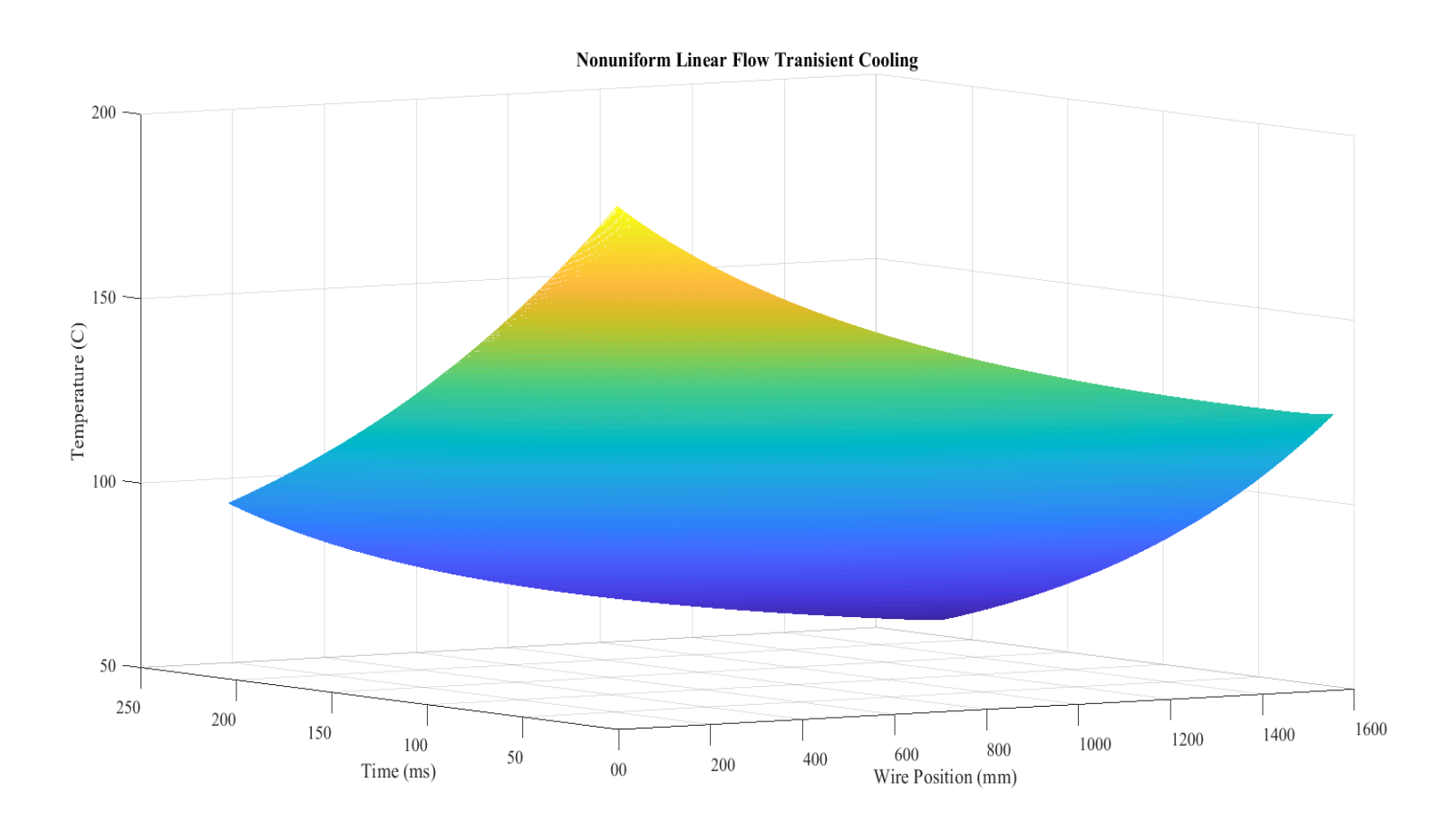


Figure 7.2. Transient Cooling with Linear Variation in Velocity,  $U_{avg}$ =10 m/s b=10 m/s

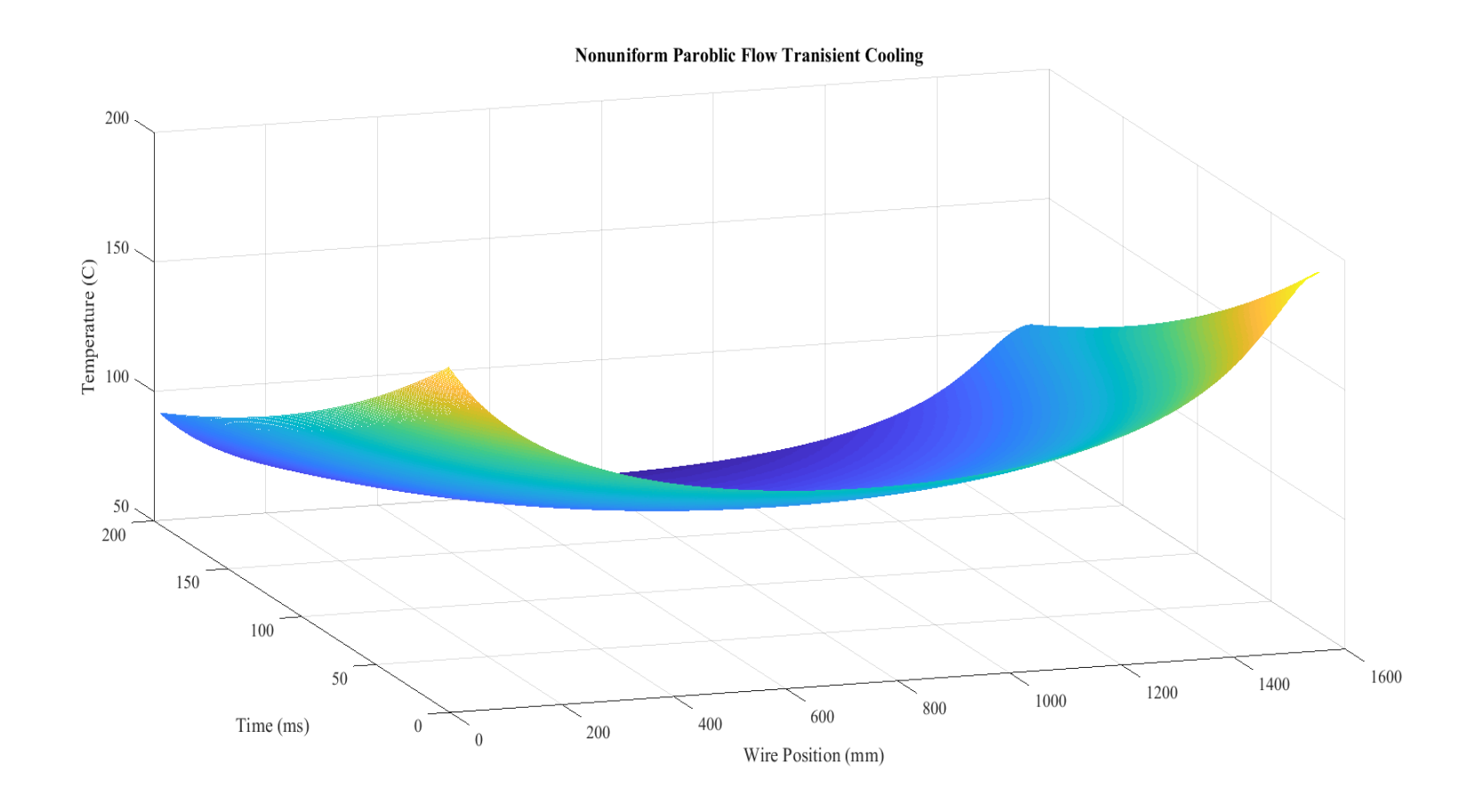


Figure 7.3. Transient Cooling with Parabolic Variation in Velocity, Shown in Equation 37

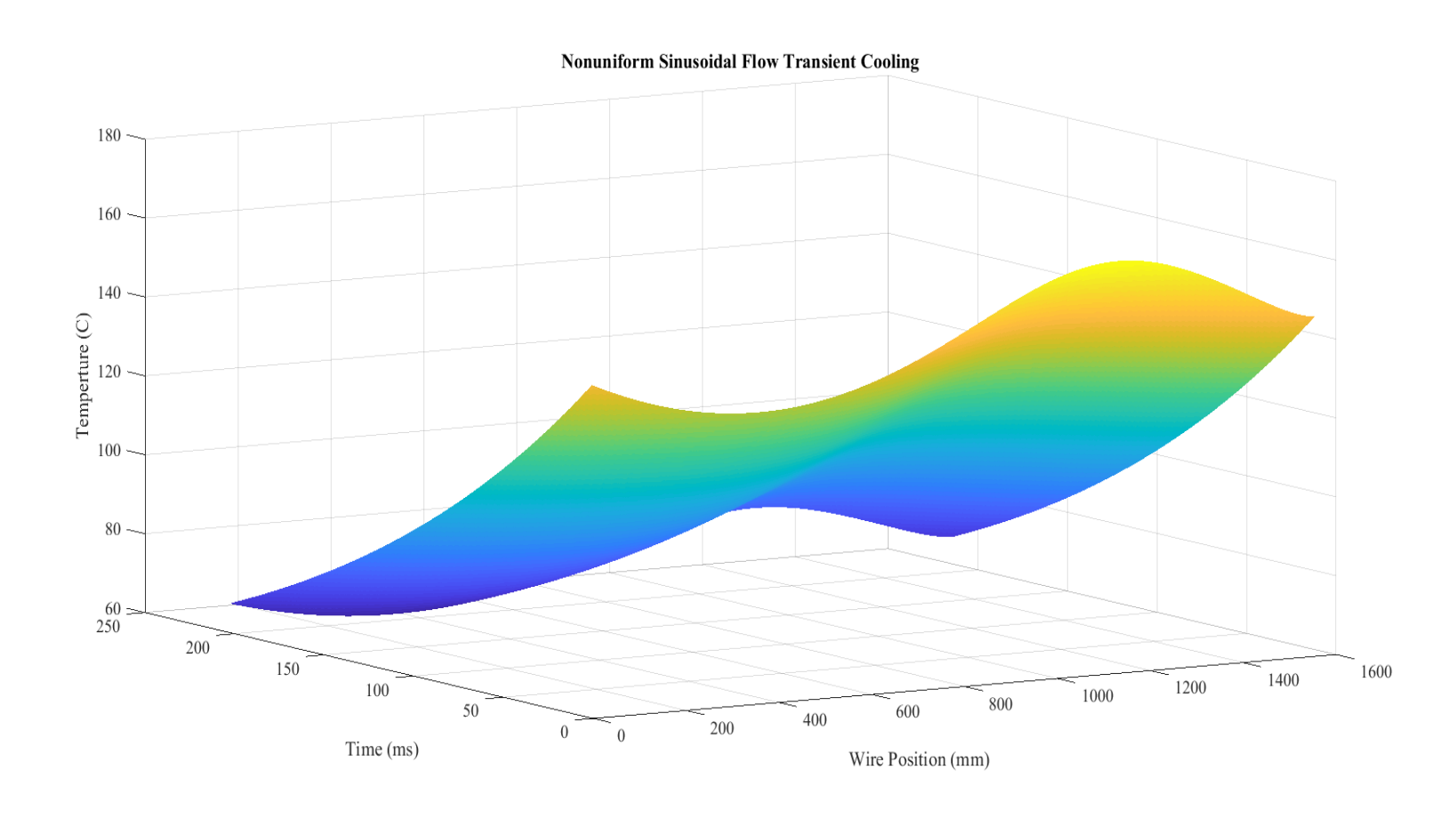


Figure 7.4. Transient Cooling with Sinusoidal Variation in Velocity, Shown in Equation 38

# Exponential Decay of Linear Velocity Profile (Average Air Speed = 10 m/s)

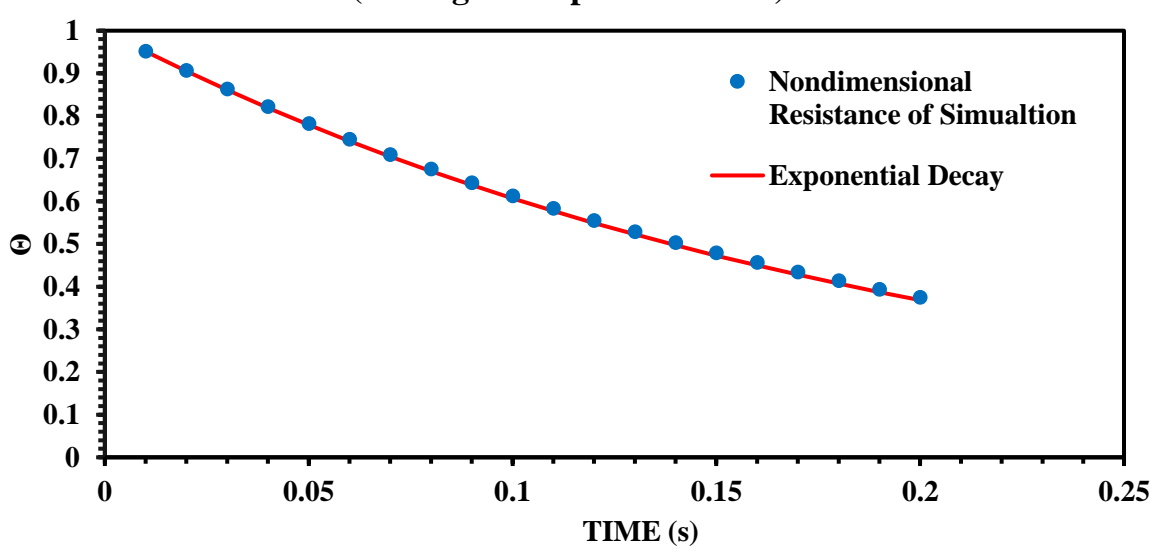


Figure 7.5. Comparison of Simulated Nondimensional Resistance to Exponential Decay with Linear Velocity Profile, Equation 36

# Exponential Decay of Parabolic Velocity Profile (Average Air Speed = 10 m/s)

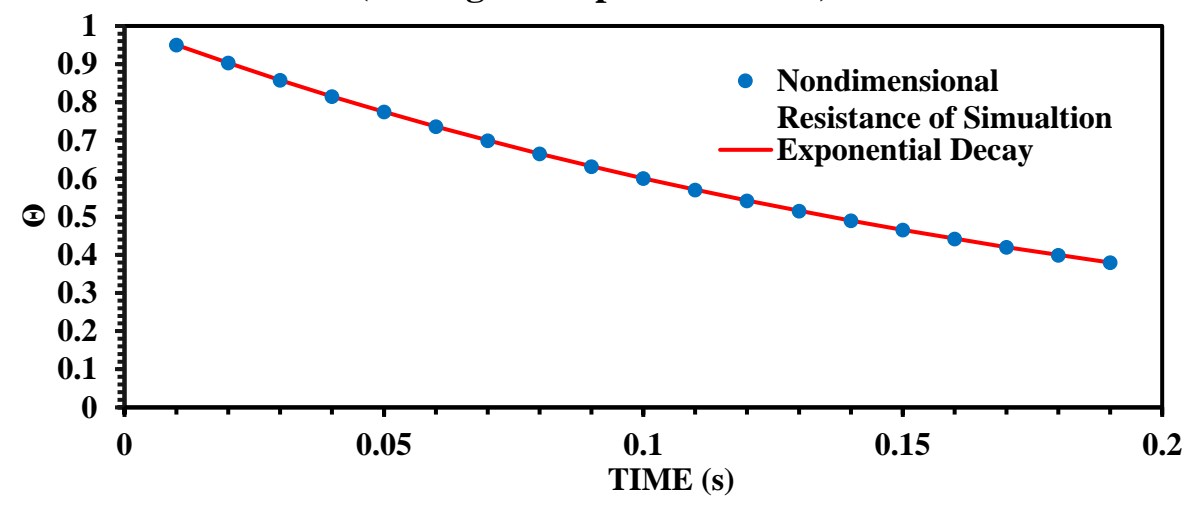


Figure 7.6. Comparison of Simulated Nondimensional Resistance to Exponential Decay with Parabolic Velocity Profile, Equation 37

# Exponential Decay of Sinusoidal Velocity Profile (Average Air Speed = 10 m/s)

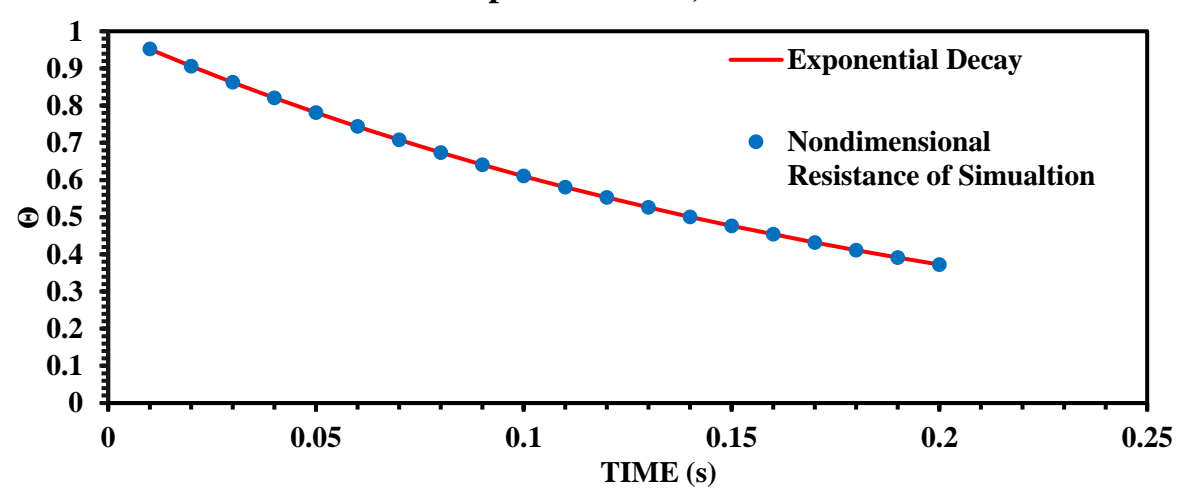


Figure 7.7. Comparison of Simulated Nondimensional Resistance to Exponential Decay with Sinusoidal Velocity Profile, Equation 38

### 7.2 Simulated Mean Velocity Prediction for Linear Variation in Velocity

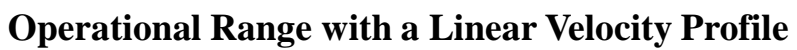
Various linear velocity profiles were used as inputs in the simulation of the temperature decay. The data for the simulation were tabulated in Table 1. Note the inferred velocity is derived from  $\tau$  and the calibration from the uniform data. As seen from these data, there were various percent difference between the mean velocity and the TTA's expected velocity (based on the uniform flow calibrations). A non-dimensional term G was introduced to relate the parameters of the velocity profile to the percent difference that was seen in the data. This non-dimensional term was then compared to the percent difference, shown in Equation 39.

$$G = \frac{1}{V_{avg}} \overline{\left| \frac{dV}{dx} \right|} H \tag{39}$$

$$\delta V = \frac{\tau_{expected} - \tau_{simulated}}{\tau_{expected}} \times 100\% \tag{40}$$

Table 7.1. Linear Flow Data

Flow Speed	G	Simulated	Mean Velocity	Inferred	Percent
Range (m/s)		Tau (sec)	(m/s)	Velocity (m/s)	Difference %
0-10	2.00	0.294	5.0	3.17	57.8
0-20	2.00	0.236	10.0	6.13	63.1
1-11	1.67	0.267	6.0	4.21	42.5
1-21	1.82	0.229	11.0	6.72	63.7
5-10	0.67	0.223	7.5	7.22	3.9
5-15	1.00	0.207	10.0	9.12	9.7
5-20	1.20	0.195	12.5	10.85	15.2
10-15	0.40	0.187	12.5	12.32	1.4
10-20	0.67	0.177	15.0	14.41	4.1
10-30	1.00	0.164	20.0	18.25	9.6
15-20	0.29	0.167	17.5	17.34	0.9



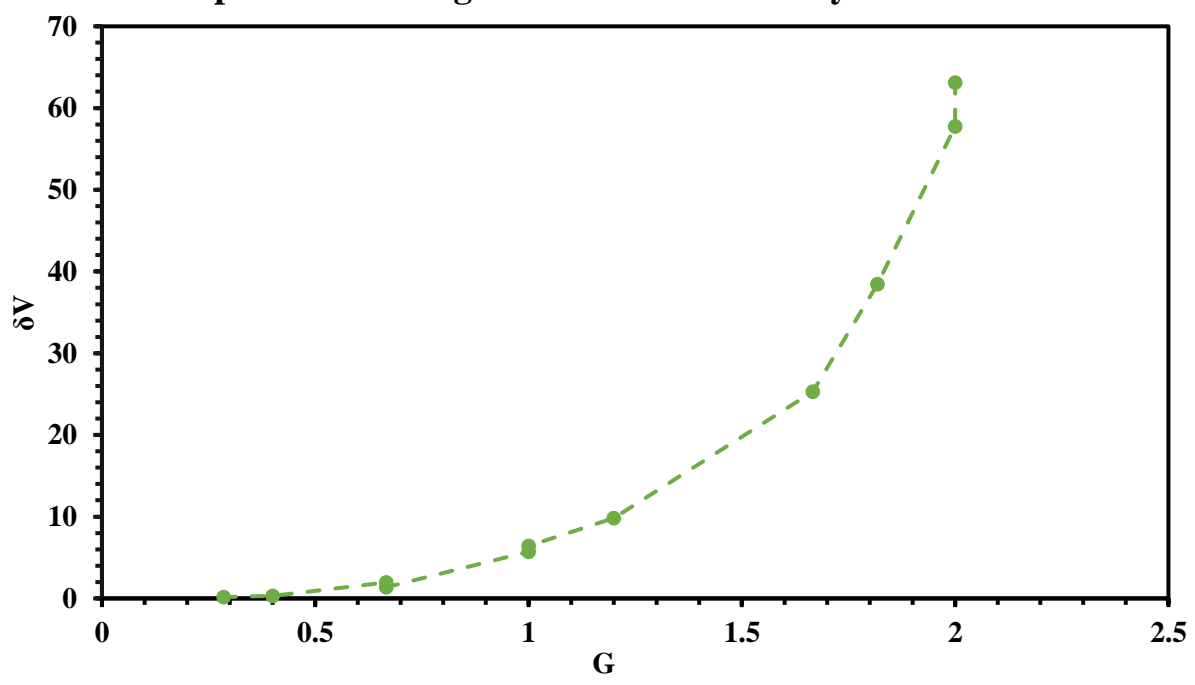


Figure 7.8. Suggested Operational Range of the TTA

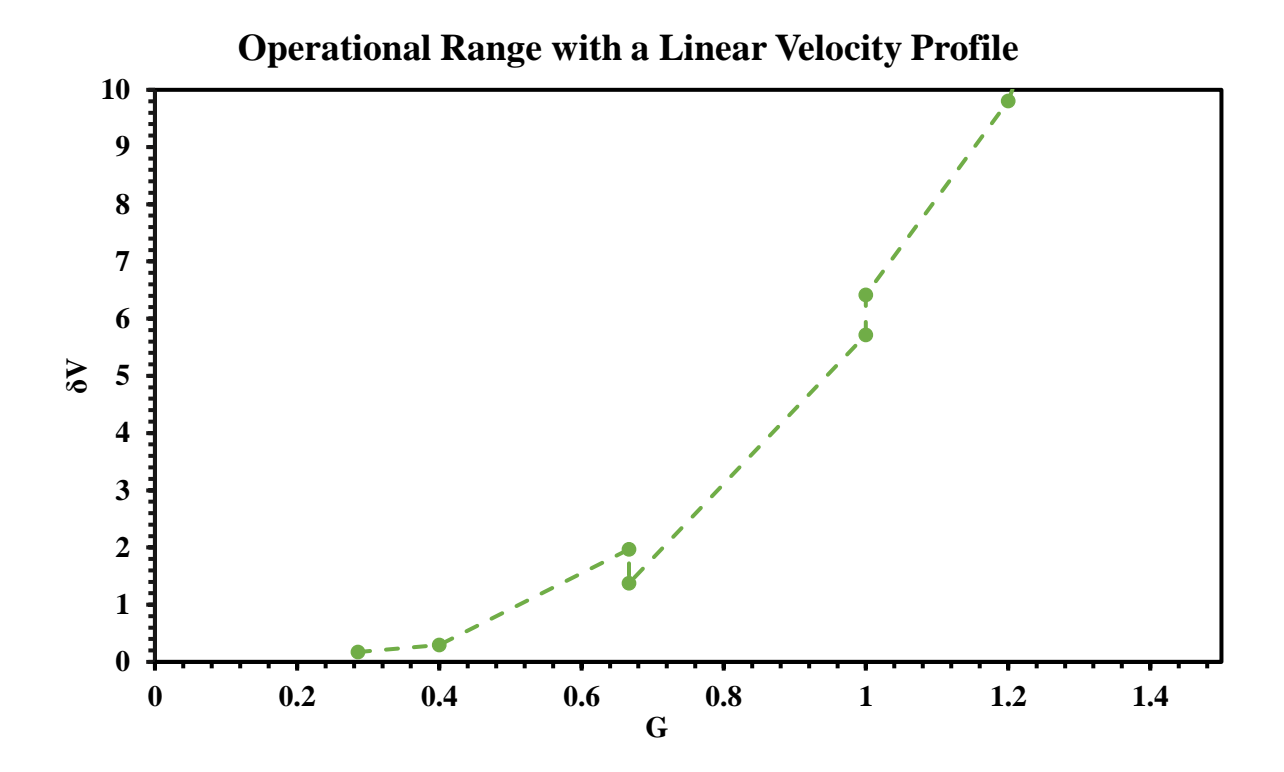


Figure 7.9. Suggested Operational Range of the TTA Zoomed In

### 7.3 Convective Heat Transfer

The non-uniform airflow was shown to differ in cooling from a uniform airflow. Specifically, the measured  $\tau$  value of the former corresponded to a smaller velocity magnitude than that of the former's spatial average. The difference between the inferred average flow and the actual average flow is the large distribution of heat convection that exist due to the non-uniform flow of air. The overall heat loss due to convections has nonlinearity, shown in Equation 41.

$$\dot{Q}_{convection} = \int_{0}^{L} h(x, t) \pi D(T_{wire}(x, t) - T_{a}) dx$$

$$= k_{a} \frac{0.981 \left(\frac{U(x)D}{v_{film}(T_{w})}\right)^{0.33} \Pr(T_{w})^{1/3}}{L} \pi D(T_{w} - T_{a})$$
(41)

The non-uniform velocity distribution causes uneven heat loss along the wire, which causes an uneven wire temperature for the first-time step of heating. This causes a change in the

convection coefficient which begins the cycle again. This will propagate the effects of the initial non-uniform velocity profile compared to the uniform velocity profile. This affects the resistance which in turn affects the  $\tau$ . A linear velocity profile from 1- 21 m/s over a straight piece of wire was used as an example. Figure 7.10 shows the initial heat convection coefficient. Figure 7.11 shows the wire temperature as it increases over time during this heating period. Figure 7.12 shows the effect of a linear velocity profile compared that of a uniform velocity distribution with the same average value(11 m/s).

### **Initial Convection Coefficient** h(x,t) (W/mK) POSITION IN THE WIRE (mm)

Figure 7.10. Initial Convection Coefficient

### **Wire Temperature Distribution with Respect to Time**

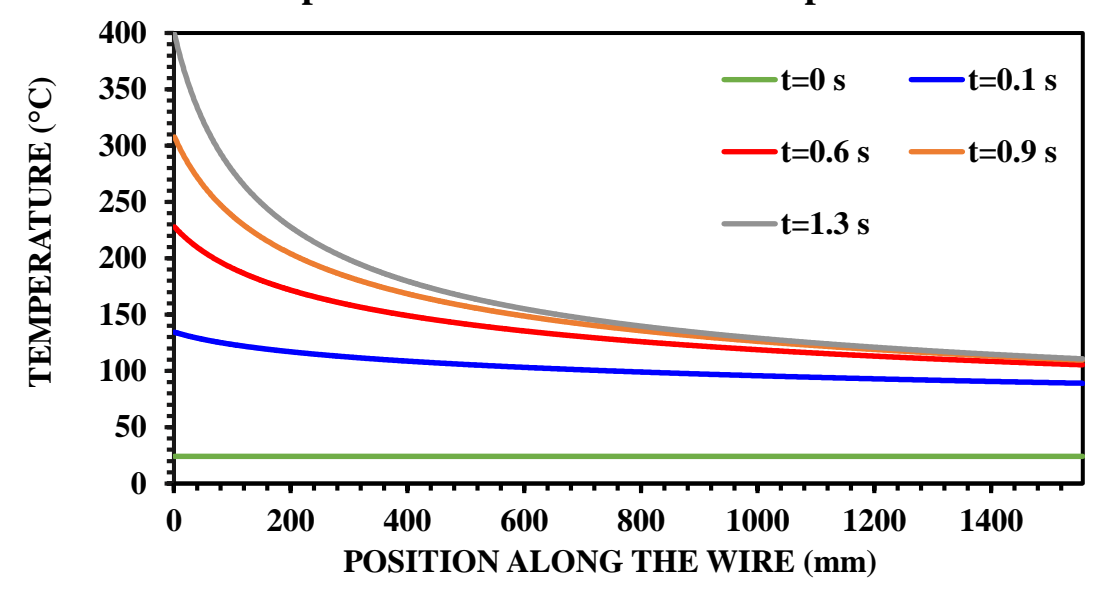


Figure 7.11. Wire Temperature Distribution with Respect to Time

# Comparison of Temperature Decay Between a Non-Uniform Velocity Profile to the Average Uniform Velocity

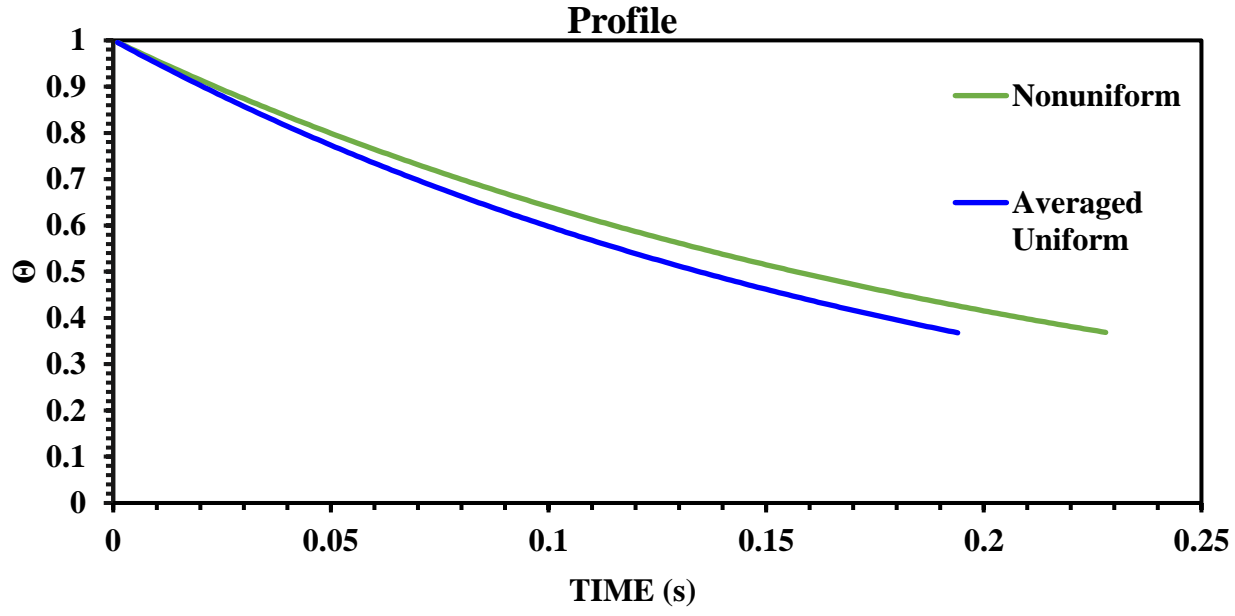


Figure 7.12. Comparison of Temperature Decay Between a Non-Uniform Velocity Profile to the Average Uniform Velocity Profile

#### 8.0 Conclusion

A TTA was built and tested to measure velocity over a cell. During calibrations the TTA and the simulation had small amounts of differences. Using the simulation, it can be determined that the TTA could operate under certain non-uniform flows. Due to the large effect of axial heat conduction, the TTA could not operate under flows with large velocity gradients or with low air speed. During testing with a vehicle, the expected speed of air over the radiator would be approximately 7.5 m/s (with a vehicle moving at 30 mph) or more. Additionally, the goal of the shroud would be to create a velocity gradient closely resembling a uniform flow, reducing the velocity gradient. This would help the flow fall into a reasonable operational range.

During a practical test inside a vehicle the TTA user could make measurements despite the error by using the tau value from the TTA and the adjacent cells. Similar to finding finite difference approximations for differential equations, the user could estimate a profile of a cell based on the adjacent cells. In the future the goal would be to find a correlation between the average air speed and the average gradient of air speed for all flow types.

**APPENDICES** 

## Appendix A. CTA Calibrations at Low Speed

## **CTA Probe Calibration at Low Air Speeds**

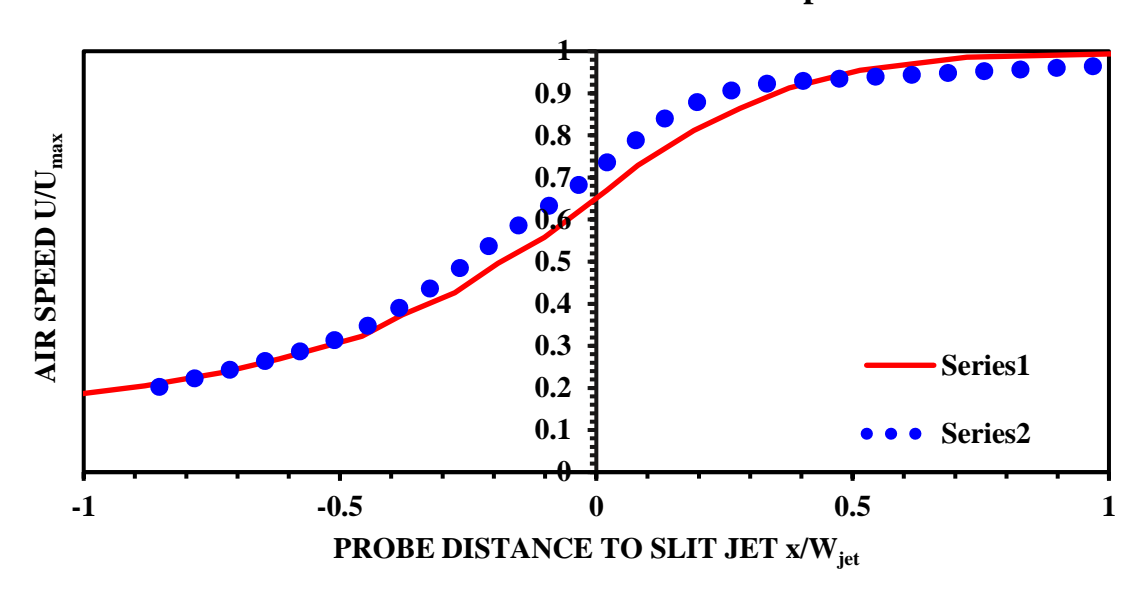


Figure A.1. CTA Probe Calibration at Low Air Speeds

### Appendix B. Calibration Curves for the Rest of the TTA

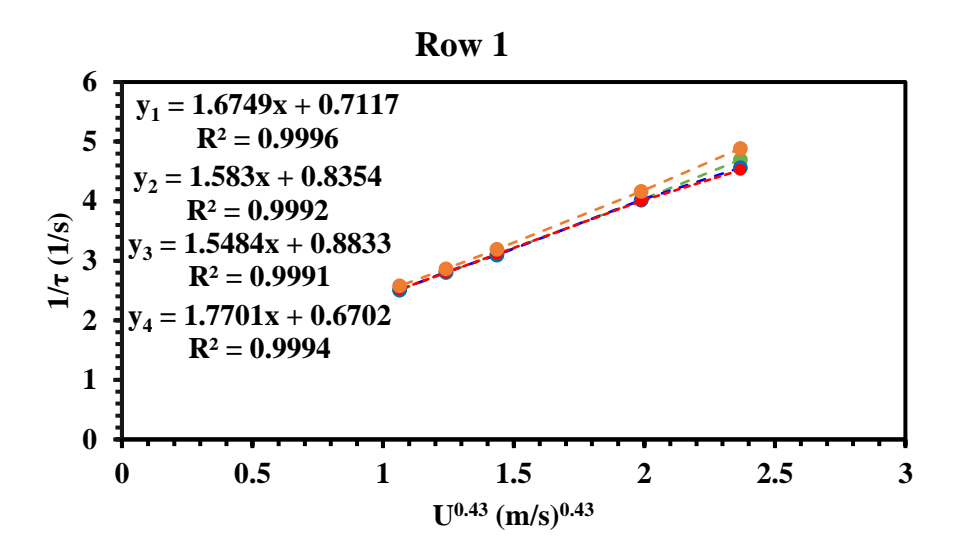


Figure A.2. Row 1 Calibration

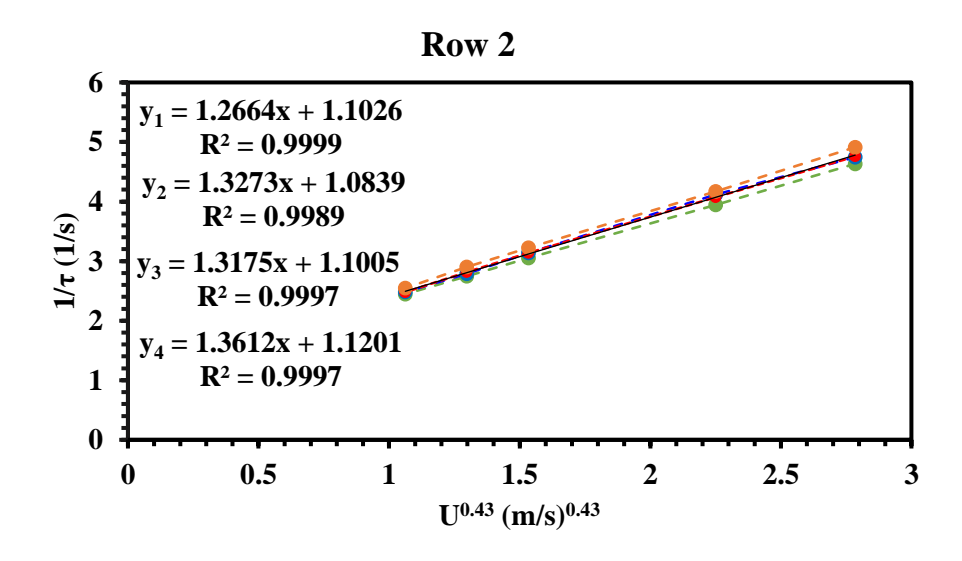


Figure A.3. Row 2 Calibration

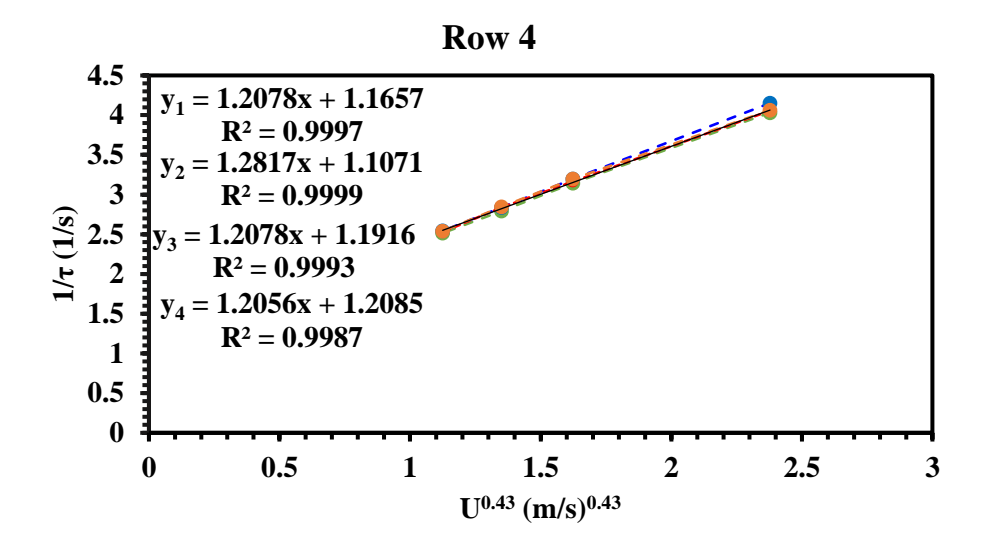


Figure A.4. Row 4 Calibration

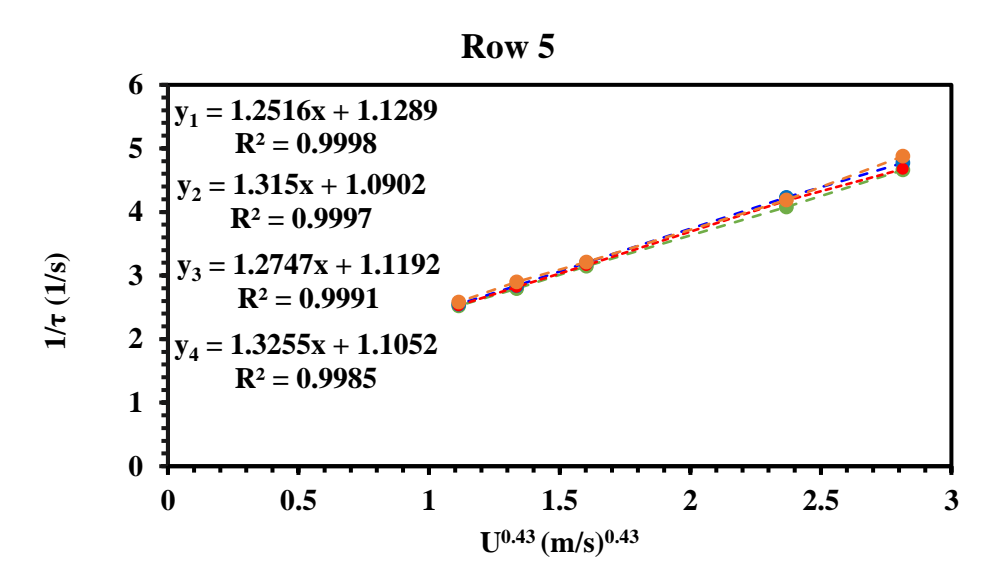


Figure A.5. Row 5 Calibration

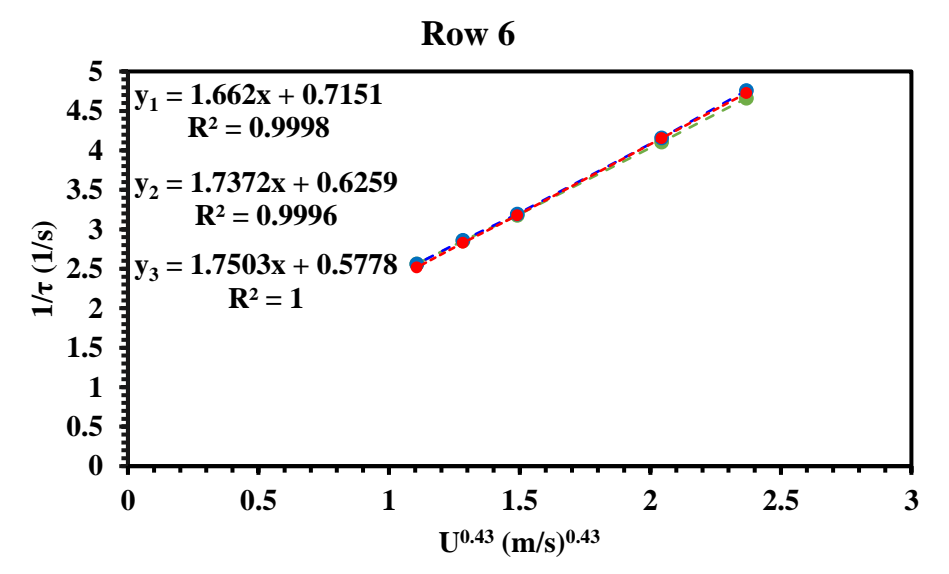


Figure A.6. Row 6 Calibration

### Appendix C. Derivation of Equations 31 and 32

The resistivity linear coefficient to temperature (Equation 5) was inserted into Equation 16.

$$\frac{k}{\rho C_p} \frac{\partial^2 T_w(x,t)}{\partial x^2} - \frac{4h}{\rho C_p D} (T_w(x,t) - T_a) + 16 \frac{I^2 * \left[ \gamma_0 \left[ 1 + \zeta \left( T_w(x,t) - T_{ref} \right) \right] \right]}{\rho C_p \pi^2 D^4}$$

$$= \frac{\partial T_w(x,t)}{\partial t}$$
(42)

$$\alpha = \frac{k}{\rho C_n} \tag{43}$$

Equation 41 was manipulated to Equation 43 or Equation 44. This is to allow the equation to be separated easier,

$$\alpha \frac{\partial^{2} T_{w}(x,t)}{\partial x^{2}} + T_{w}(x,t) \left[ \frac{16I^{2} \alpha \gamma_{0} \zeta}{k\pi^{2} D^{4}} - \frac{4h\alpha}{kD} \right] + \left[ \frac{4h\alpha T_{a}}{kD} + \frac{16I^{2} \alpha \gamma_{0}}{k\pi^{2} D^{4}} \left( 1 - \zeta T_{ref} \right) \right]$$

$$= \frac{\partial T_{w}(x,t)}{\partial t}$$

$$(44)$$

$$\alpha \frac{\partial^2 T_w(x,t)}{\partial x^2} + \nu T_w(x,t) + \alpha = \frac{\partial T_w(x,t)}{\partial t}$$
 (45)

BC1: 
$$\frac{\partial T(0,t)}{\partial x} = 0$$
 BC2:  $\frac{\partial T(L,t)}{\partial x} = 0$  IC:  $T_w(x,t=0) = F(x)$ 

The equation is separated into a steady state part and a transient part.

$$T_w(x,t) = w(x,t) + u(x)$$
(46)

$$\alpha \frac{d^2 u(x)}{dx^2} + vu + a = 0 \tag{47}$$

BC1: 
$$\frac{du(x)}{dx}\Big|_{x=0} = 0$$
 BC2:  $\frac{du(x)}{dx}\Big|_{x=L} = 0$  (48)

After integrating and applying boundary conditions it shows that the steady state is constant which is expected with uniform flow (the point where the energy from heat generation balances the energy from the heat loss due to convection).

$$u(x) = -\frac{a}{v} \tag{49}$$

The transient part of the Equation 45 is evaluated below

$$\frac{\partial w}{\partial t} = \alpha \frac{\partial^2 w}{\partial x^2} + \nu w \tag{50}$$

BC1: 
$$\frac{\partial w}{\partial x}\Big|_{x=0} = 0$$
 BC2:  $\frac{\partial w}{\partial x}\Big|_{x=L} = 0$  IC:  $w(x, t = 0) = F(x) + \frac{a}{v}$ 

The transient part is broken down even further to special variable and time variable.

$$w(x,t) = X(x)\Gamma(t) \tag{51}$$

$$\Gamma'X = \alpha \Gamma X'' + \nu \Gamma X \tag{52}$$

$$\frac{1}{\alpha} \left( \frac{\Gamma'}{\Gamma} - \nu \right) = \frac{X''}{X} = -\lambda^2 \tag{53}$$

$$\Gamma(t) = C_3 \exp(-(\alpha \lambda^2 - \nu)t)$$
 (54)

$$X(x) = C_4 \sin(\lambda x) + C_5 \cos(\lambda x) \tag{55}$$

BC1: 
$$\frac{dX(x=0)}{dx} = 0$$
 BC2: 
$$\frac{dX(x=L)}{dx} = 0$$

The boundary condition was applied to get the eigen condition.

$$\lambda_n = \frac{n\pi}{L} \quad n = 0, 1, 2 \dots \tag{56}$$

The special component (50) and the time (49) component combine, their constants were merged to get  $C_n$ .

$$w(x,t) = \sum_{n=0}^{\infty} C_n \cos\left(\frac{n\pi x}{L}\right) \exp(-(\alpha \lambda^2 - \nu)t)$$
 (57)

$$C_n = \frac{2}{L} \int_0^L \left[ F(x) + \frac{a}{\nu} \right] \cos\left(\frac{n\pi x}{L}\right) dx \tag{58}$$

$$T_w(x,t) = -\frac{a}{\nu} + \frac{2}{L} \sum_{n=0}^{\infty} \int_0^L \left[ \left( F(x) + \frac{a}{\nu} \right) \cos\left(\frac{n\pi x}{L}\right) dx \right] \cos\left(\frac{n\pi x}{L}\right) \exp(-(\alpha \lambda^2 - \nu)t)$$
 (59)

The initial condition is substituted for F(x)

$$T_{w,linear}(x,t=0) = \frac{20x}{L} + T_a$$
 (60)

$$C_0 = 10 + T_a + \frac{a}{v} \tag{61}$$

$$C_n = \frac{20L(\cos(n\pi) - 1)}{n^2\pi^2} \quad n = 1, 2, 3 \dots$$
 (62)

 $T_{w,linear}(x,t) =$ 

$$-\frac{a}{\nu} + \sum_{n=1}^{\infty} \left[ \frac{40(\cos(n\pi) - 1)}{n^2 \pi^2} + 10 + T_a + \frac{a}{\nu} \right] \cos\left(\frac{n\pi x}{L}\right) \exp(-(\alpha \lambda^2 - \nu)t)$$
 (63)

$$T_{wire,parabolic}(x,t=0) = -40x^2 + 40x + T_a$$
 (64)

$$C_0 = \frac{100}{3} + T_a + \frac{a}{v} \tag{65}$$

$$C_n = \frac{-40L(\cos(n\pi) + 1)}{n^2\pi^2} \quad n = 1, 2, 3 \dots$$
 (66)

 $T_{w,parabolic}(x,t) =$ 

$$-\frac{a}{\nu} + \sum_{n=1}^{\infty} \left[ \frac{-80(\cos(n\pi) + 1)}{n^2 \pi^2} - \frac{40L}{3} + 20 + T_a + \frac{a}{\nu} \right] \cos\left(\frac{n\pi x}{L}\right) \exp(-(\alpha \lambda^2 - \nu)t)$$
(67)

REFERENCES

#### REFERENCES

- Boetcher, S. K. (2014). Natural Convection from Circular Cylinders. Cham: Springer. [1]
- Bruun, H.H. (1995). Hot-wire Anemometry. Oxford University Press. [2]
- Carslaw, H., Jaeger, J., (2011) Conduction of Heat in Solids. Clarendon Pr. [3]
- "ClearMechanic: Professional Mobile Inspections for Technicians, Mechanics,
  Automotive Experts, Dealer Service Centers and Repair Shops ClearMechanic.com,"
  ClearMechanic: Professional Mobile Inspections for Technicians, Mechanics,
  Automotive Experts, Dealer Service Centers and Repair Shops ClearMechanic.com,
  clearmechanic.com/. [4]
- Hahn, D., Ozisik, M. (2012). Heat Conduction. Wiley. [5]
- Foss, J., Peabody, J., Norconk, M., Lawrenz, A. (2006), "Ambient temperature and free stream turbulence effects on the thermal transient anemometer". *Measurement Science & Technology*, Vol. 17, pp. 2519-2526. [6]
- Foss, J., Schwannecke, J., Lawrenz, A., Mets, M., Treat, S., Dusei, M. (2004). "The thermal transient anemometer". *Measurement Science and Technology*. Vol. 15, pp. 2248. [7]
- Incropera, F. P., DeWitt, D. P. (2007). Fundamentals of heat and mass transfer. J. Wiley. [8]
- Morris, S., Foss, J. (2003). "Transient thermal response of a hot-wire anemometer". *Measurement Science and Technology*. Vol. 14, pp. 251. [9]